NASA Technical Memorandum 73278

GEOS-3 Coherent C-Band Tracking Data Reduction and Analysis

W. B. Krabill
K. L. Borman

September 1978

National Aeronautics and Space Administration

Wallops Flight Center
Wallops Island, Virginia 23337
AC 804 824-3411

National Aeronautics and
Space Administration

Wallops Flight Center
Wallops Island, Virginia
23337

NASA

Reply to Attn of: TL (A-13)

OCT 2 1978

NASA Scientific and Technical
Information Facility
Attn: Acquisitions Branch
Post Office Box 8757
Baltimore/Washington International
Airport, MD 21240

Subject: Document Release for NASA TM-73278

Document Release Authorization Form FF 427 and two (2) copies of the following report are forwarded:

NASA TM-73278 GEOS-3 Coherent C-Band Tracking Data Reduction and Analysis.

We are forwarding, under separate cover, thirty (30) additional copies of NASA TM-73278.

James C. Floyd

James C. Floyd
Head, Administrative Management Branch

Enclosures

NASA Technical Memorandum 73278

GEOS-3 Coherent C-Band Tracking Data Reduction and Analysis

W. B. Krabill
Wallops Flight Center
Wallops Island, Virginia 23337

and

K. L. Borman
Washington Analytical Services Center, Inc.
6801 Kenilworth Avenue
Riverdale, Maryland 20840

National Aeronautics and
Space Administration

Wallops Flight Center
Wallops Island, Virginia 23337
AC 804 824-3411

ACKNOWLEDGEMENTS

The authors wish to thank the large number of people who have advised, assisted, and otherwise contributed to the work reflected in this report. Special acknowledgment must be given to the indispensable efforts of Chuck Davis and Al Selser at Wallops Flight Center, Chreston Martin at EG&G/Wolf, and Don Dempsey of the RCA Surface and Missile Radar Division, all of whom brought to bear their substantial and invaluable experience in the operation and calibration of C-Band radars.

TABLE OF CONTENTS

SECTION 1.0
INTRODUCTION

The GEOS-3 spacecraft, launched April 10, 1975, was the first orbiting vehicle to carry a coherent C-Band transponder. The previous spacecraft in the GEOS series carried non-coherent C-Band transponders, which were not suitable for two-way Doppler range rate measurement.

Approximately one-third of the C-Band radars available to support the GEOS-3 mission have coherent capability, either the Coherent Signal Processor (CSP) or Velocity Extraction Subsystem (VESS). These systems produce a digital measurement of target range-rate along the slant range vector. The measurement system is implemented as an additional Type II servo, modeling $\dot{R}$ and $\ddot{R}$ and driven by error signals extracted from return signal frequency shift compared to the local oscillator, with suitable provisions for resolving harmonic ambiguity.

Prior to the launch of GEOS-3, these systems were able to produce range rate data on orbiting vehicles only when the radar was operated in the skin track mode. This data was characterized by severe noise and signal strength problems. The advent of a spacecraft-borne coherent transponder allowed the examination of precise C-Band range rate data in the context of a trajectory highly constrained by orbit dynamics. The general quality of this data is illustrated by Figure 1-1, showing range rate residuals for a single GEOS-C pass taken by the AN/FPQ-6 radar at Wallops Island, Virginia. The residuals are about an orbit fit to the range and angle data taken by the radar. This data shows low noise (0.65 cm/sec RMS) and little systematic error after correction in the data reduction process for known timing and measurement bias errors. The identification and elimination or reduction of these errors is the subject of this report.

FIGURE 1–1. GEOS–3 COHERENT RANGE RATE RESIDUALS
REV 9799 WALLOPS AN/FPQ–6
RMS .95 CM/SEC

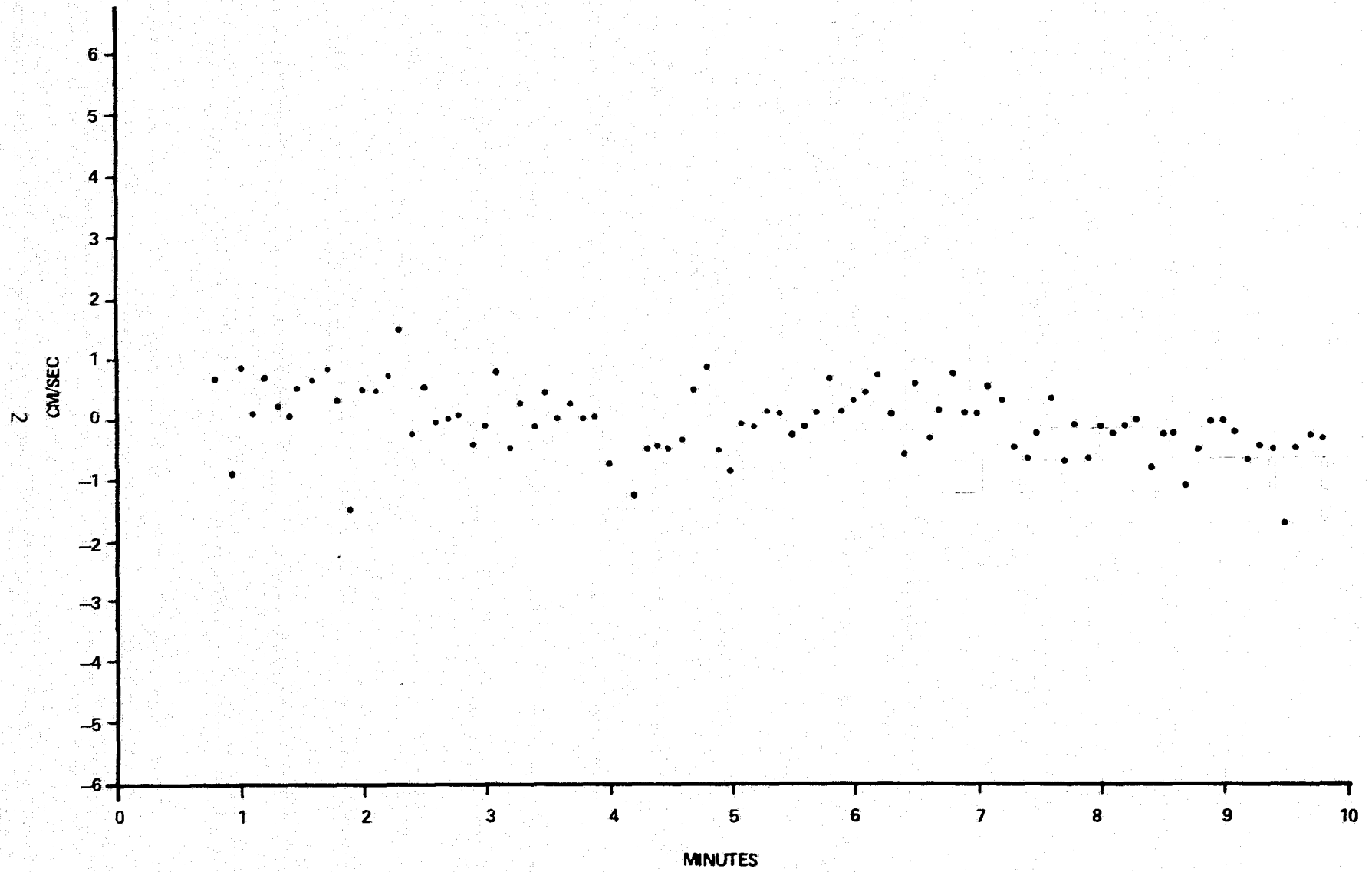

The availability of two independent data sets simultaneously from the same instrument suggested that calibration efforts might be enhanced by the ability to compare them in the same measurement domain. The idea of integrating range rate data into pseudo range measurements is not new; a similar study was undertaken in support of GEOS-2 by Wells and Guard (1). Their results were severely limited by the fact that only range rate data from the skin tracking mode was available. Using this work as a foundation, we have extended the technique using the more precise range rate data available from the GEOS-3 coherent transponder.

Results from the integrated range evaluation led to the development of additional corrections to the conventional C-Band ranges, leading to a reduction both in noise and systematic error. These techniques include:

- Filtering of data to reduce relatively high radar recording rates (10 or 20 pps) to convenient rates for orbital data reduction (usually 1 point per 6 seconds).

- A radar AGC based correction for beacon delay variations with signal strength.

The former reduced typical RMS range noise figures for the Wallops Island FPQ-6 from one meter or more to the 25-50 cm range, while the latter corrected for a systematic error whose dynamic range through a typical pass can approach 2 meters.

SECTION 2.0
PROCESSING TECHNIQUES

This section details the processing techniques used to produce and analyze the integrated Doppler range data, including the preprocessing corrections necessary to the conventional* ranges produced by the radar, which define the reference orbit for evaluation of integrated range results. The overall data processing organization is shown in Figure 2-1.

All of the data presented in this report were obtained by the AN/FPQ-6 radar at Wallops Island, Virginia. This radar is equipped with the Coherent Signal Processor pulse Doppler modification and a DIRAM range machine. Tracking data is recorded digitally in real-time under control of the radar's RCA 4101 computer. The remainder of the data processing activities were carried out at the Wallops Flight Center Information Processing Laboratory, on either the Honeywell 625 or Honeywell 635 medium scale computer systems.

The initial step in the processing chain was the reformatting of the binary site tapes into a form compatible with the 625/635 computer system. This step is undertaken by the PASS1 program. The output of this program is then input into the PASS2 C-Band preprocessor. It is within this program that the filtering, integration, and other calibration techniques discussed in this report were implemented. The output of the PASS2 program, consisting of the final reduced and corrected data, was then used in the orbit determination program GEODYN. Resulting residual information was passed to a residual analysis program GEORGE, which was modified to incorporate appropriate integrated range error models. In parallel to this sequence, the ORAN error analysis program was used to predict the effects of the various modeled and unmodeled errors on the batch least squares orbital solution.

*In the case of the Wallops Island AN/FPQ-6 these are often referred to as DIRAM ranges, after the DIgital RAnge Machine, which is the range tracker on that radar.

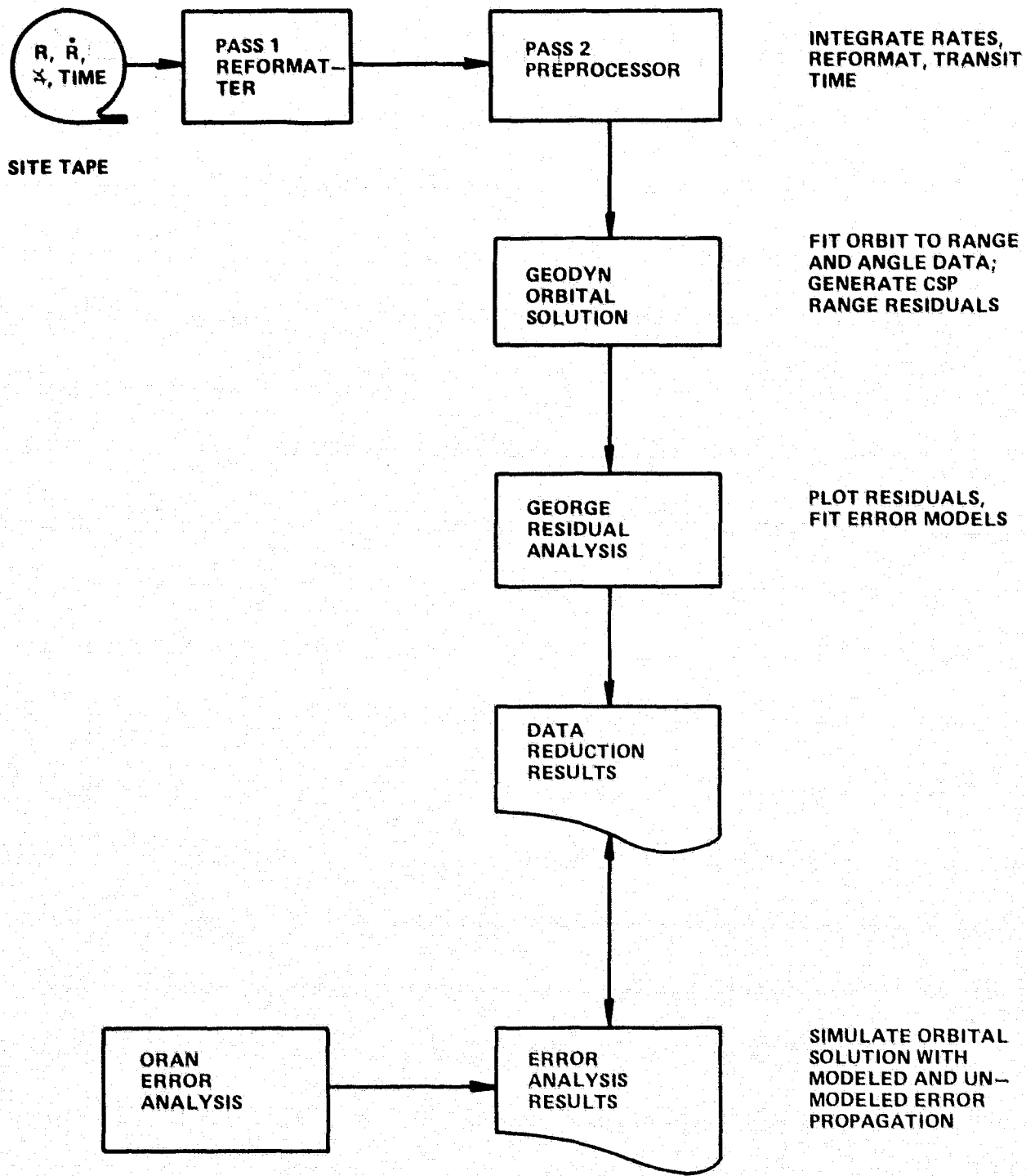

FIGURE 2-1. INTEGRATED RANGE PROCESSING AND ANALYSIS

The relevant portions of each of these processing steps are discussed individually in the following sections.

2.1 INTEGRATED DOPPLER RANGES

The range rate measurements at the radar sampling rate of 10 or 20 pps are numerically integrated with a simple trapezoid rule integration scheme formulated as,

$$R_i = R_{i-1} + \frac{\dot{R}_i + \dot{R}_{i-1}}{2} \Delta t$$

This scheme is graphically illustrated in Figure 2-2. Despite its simplicity, this algorithm has several advantages. In particular, it

- does not require equally spaced samples in time,
- is fast and efficient computationally, and
- has error dependent on the second derivative of the integrand (here $\ddot{R}$), i.e., the non-linearity of the function to be integrated between consecutive data points.

In general, this scheme has been found adequate for the study at hand. The function (range rate) is sampled frequently enough (10 or 20 pps) in relation to the magnitude of the dominant error term ($\ddot{R}$) to limit integrator error to a few cm in magnitude. A more complete analysis of the integration technique is included in this report as Section 2.4.2.

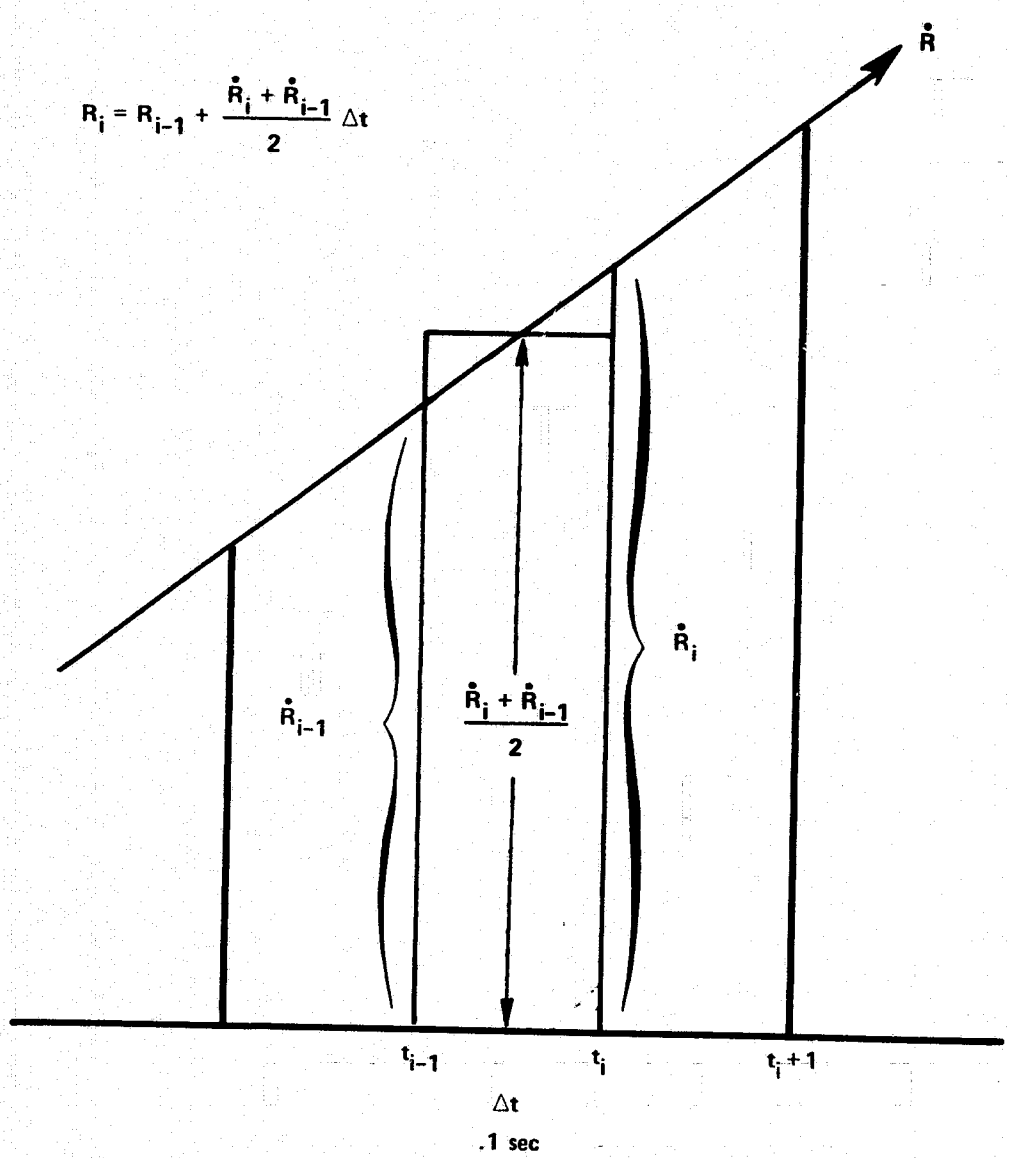

FIGURE 2-2. NUMERICAL INTEGRATION FUNCTION

The determination of the constant of integration, which in this case amounts to a "zero-set" or bias correction for the integrated ranges, is initially accomplished by adjusting them in a batch sense to the ensemble of DIRAM ranges. The integration process is begun using the DIRAM range associated with the first valid range rate measurement. As the process progresses, the sum of the differences between the integrated Doppler range and DIRAM range at each point is kept. At the end of the pass the ensemble of integrated ranges is corrected by the mean difference, i.e.,

$$\frac{1}{n} \sum_{1}^{n} (R_{c_i} - R_{d_i})$$

where

R_{c_i} = ith C-Band DIRAM Range

R_{d_i} = ith integrated Doppler Range

In effect this introduces into the integrated range data set a bias identical to that in the DIRAM range machine.

The integrated ranges are sampled at every 60th point for an output data rate of once every 6 seconds. This is a convenient rate for data in orbital solutions and corresponds to that chosen for reduction of normal range, range rate, and angle data. Because of the low noise on the data, there is minimum benefit to be gained by filtering the integrated ranges.

It should be noted that prior to the integration process, range rate data is corrected for bias using an estimate determined by a pre- and post-mission "one line up - one line down" calibration procedure, which is further discussed in Section 3.0. Additionally, measurement time tags are corrected for propagation delay and the data is reformatted suitably for input to an orbit determination program.

2.2 DIRAM RANGE CORRECTIONS

The principal preprocessing corrections now made to the DIRAM ranges, in the order of their development and implementation, are

- Bias adjustment based on pre- and post-mission ranging to a surveyed target.
- 60 to 1 reduction of sampling rate through application of a polynomial midpoint filter.
- Correction for within pass beacon delay variation based on radar receiver AGC.

The first of these, bias correction based on pre- and post-mission ranging to a surveyed target, is a conventional technique long used in a great many ranging systems. The Wallops Island FPQ-6, with suitable pre-mission warmup time, does not drift significantly in range bias during the mission interval. The remaining corrections were first implemented during the GEOS-3 study, and are discussed individually.

2.2.1 Filtering

C-Band radars typically record data at either 10 or 20 pps, a considerably greater rate than is necessary or useful for orbit determination and geodetic studies. Historically this data has been reduced by sampling; i.e., the often used once-per-six-second data rate was achieved by selecting every 60th or 120th point and ignoring the rest. It was felt that a relatively simple filtering technique might considerably reduce the noise of the resultant data. The intent was not to derive an optimal or near optimal filter or smoother for the range data, but rather to find a simple and computationally efficient method to stop "wasting" most of the information recorded.

The solution implemented was to apply a quadratic polynomial midpoint filter to each set of 60 or 120 points. Serial correlation effects are minimal since the filter is not applied recursively but rather to each successive six second interval of data. In effect, it is simply a one higher order technique than averaging each consecutive set of 60 points. Moreover, the filter is implemented as a set of 60 weighting coefficients, which does not add significantly to the computational burden of preprocessing the large amounts of C-Band data processed at Wallops Flight Center. Figures 2-3 and 2-4 show the results of filtering on a typical range data pass.

2.2.2 Beacon Delay Variation

Both the coherent and the non-coherent C-Band transponders on the GEOS-3 spacecraft were the subject of detailed prelaunch calibration and test procedures as reported by SELSER (2). Figure 2-5, excerpted from his report shows the delay variation of the coherent transponder with received signal strength. In the case of the AN/FPQ-6 at Wallops Island, with the normal GEOS-3 setup, received signal strength at the spacecraft transponder can vary over the range -40 to -30 dBM within a single pass as the range varies from almost 3,000 Km at 5° elevation to less than 1,000 Km at high elevation angles. As the figure illustrates, this causes a variation of approximately 6ns in two-way propagation delay or a change of over a meter in the radar measured range. This significant systematic effect was uncorrected in the past due largely to the difficulty of extracting transponder received signal strength information from the spacecraft TM stream and suitably correlating it with the C-Band data processing effort. Nevertheless, proper evaluation of the extremely low noise integrated Doppler ranges could not be completed with a systematic error of this magnitude in the ranges determining the reference orbit. Accordingly, a scheme was developed whereby the digitized AGC level at the tracking radar could, with suitable calibrations, be converted to radar received signal to noise ratio, and ultimately, through the radar equation and knowledge of the radar's and spacecraft's transmitted power, to spacecraft transponder received signal strength and finally, beacon delay variation. This process is illustrated in Figure 2-6.

FIGURE 2–3. UNFILTERED GEOS–3 DIRAM RANGE RESIDUALS
REV 9799 WALLOPS AN/FPQ–6
RMS 1.35 M

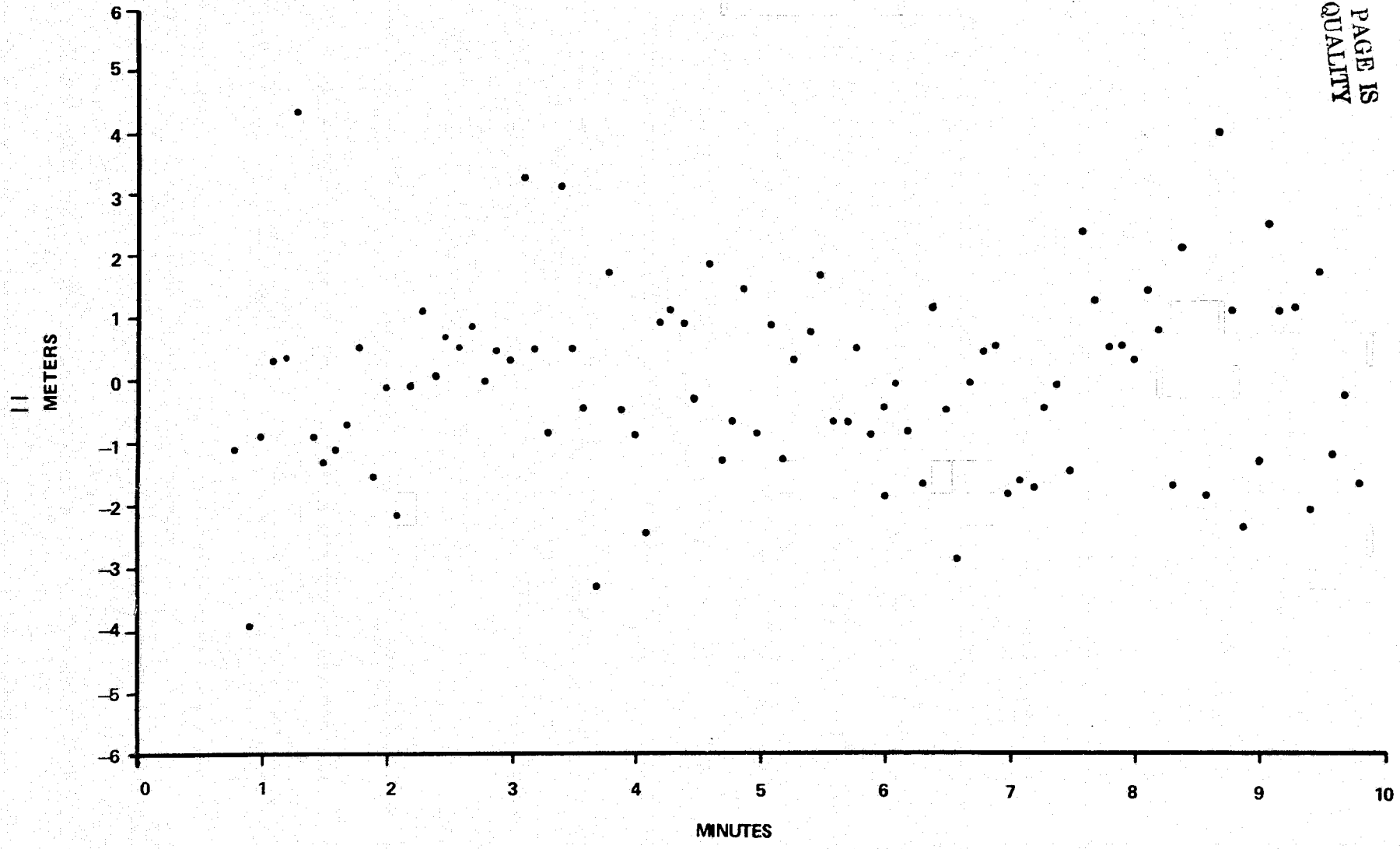

FIGURE 2–4. FILTERED GEOS–3 DIRAM RANGE RESIDUALS

REV 9799 WALLOPS AN/FPQ–6

RMS 38 CM

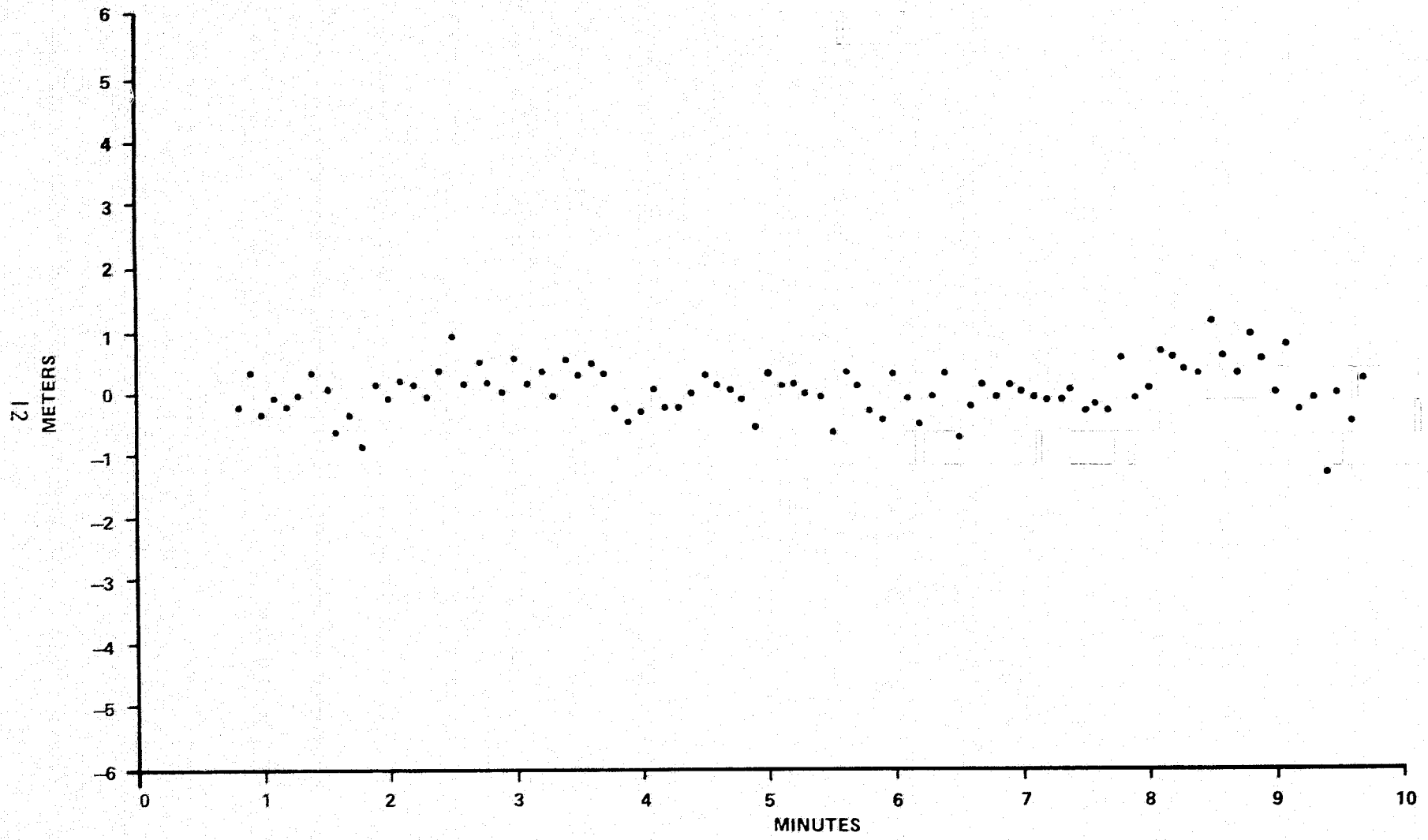

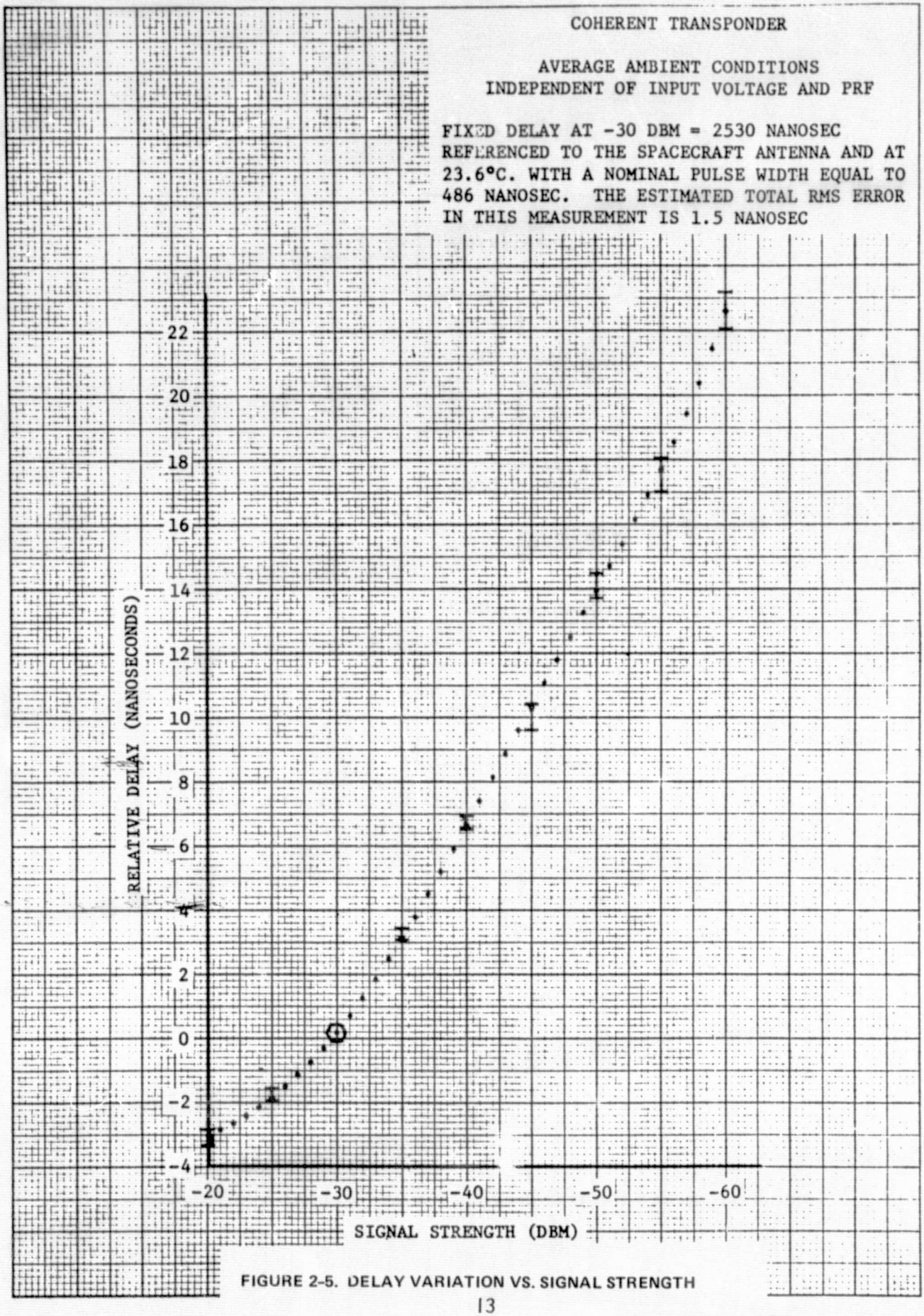

FIGURE 2-5. DELAY VARIATION VS. SIGNAL STRENGTH

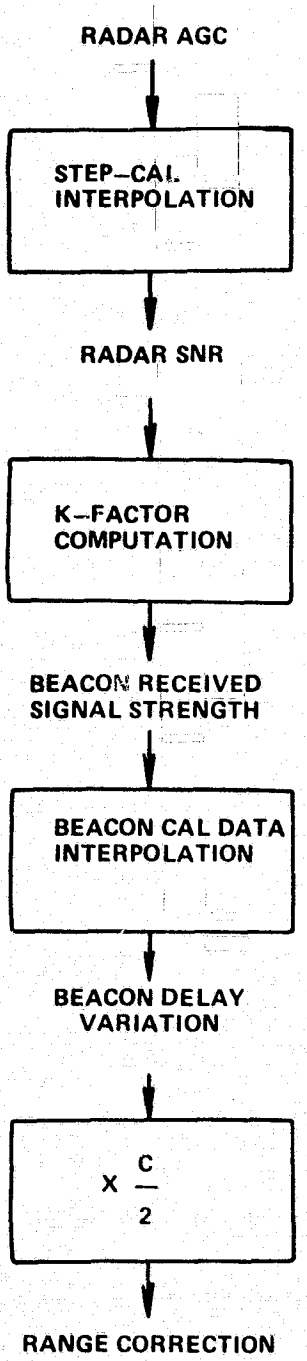

FIGURE 2-6. RADAR AGC BEACON DELAY VARIATION CORRECTION PROCESS

Initially the radar performs an AGC-stepcal procedure which functionally relates the radar recorded AGC level to the radar received signal-to-noise ratio. The radar AGC from each point during tracking can then be converted, through a table-lookup linear interpolation process, to radar received SNR. This in turn can be converted to transponder received signal strength through a K-factor computation (Figure 2-7) making use of the radar equation and knowledge of radar and transponder operating parameters.

Finally, beacon received signal strength is converted to relative delay by another table-lookup linear interpolation based upon the pre-mission test results reported by SELSER. The scheme is implemented with a relative beacon delay of 0 (i.e., nominal delay of 379.48 m) at the -30 dB beacon received signal strength level.

2.3 ORBIT DETERMINATION

Reference orbits for all of the analyses reported here are single station, single pass trajectories fit to the DIRAM range and angle data from each radar pass. The orbit determination program used was the GEODYN program (3).

Single station single pass orbital solutions almost always fit very well, the orbit largely accomodating most systematic errors, particularly station position errors and absolute timing errors which are near unobservable in data from a single station. This method for determining the reference trajectory for integrated range analyses was chosen specifically for these reasons. The low noise integrated Doppler ranges would be very sensitive to almost all such unmodeled errors. By using a reference trajectory determined by an identically colocated station using a common timing standard and position, timing and gravity model errors are essentially eliminated. Furthermore, tropospheric refraction correction error, identical for both sets of ranges, is largely accomodated by the orbit. The remaining systematic errors observable in the integrated range residuals about such a reference orbit are listed in Table 2-1.

FIGURE 2-7. K-FACTOR COMPUTATION

RECEIVER — WALLOPS ISLAND AN/FPQ–6

P_R = 2.2 Mw

L_{DR} = 2.3 db

B = 2.4 MHz

F_o = 4 db

TRANSMITTER — GEOS-3 VEGA COHERENT BEACON

P_t = 130 w

L_{UR} = 2.6 db

ENVIRONMENT

K = 1.38×10^{-20}

T_o = 290^o K

$$SS = \frac{P_R G_R G_T \lambda^2}{(4\pi)^2 R^2 L_{UR} L_{UA} L_{UT}}$$

$$SNR = \frac{P_T G_T G_R \lambda^2}{(4\pi)^2 R^2 L_{DT} L_{DA} L_{DR} K T_o B F_o}$$

$$K_B = \frac{SS}{SNR} = \frac{P_R L_{DR} K T_o B F_o}{P_T L_{UR}}$$

K_B = – 64.2 dbm

SS (dbm) = SNR (db) – 64.2

TABLE 2–1.

INTEGRATED RANGE ERROR SOURCES

A. ERRORS VISIBLE IN INTEGRATED RANGE RESIDUALS

I. SYSTEMATIC ERRORS IN RANGE AND ANGLE DATA USED TO DETERMINE THE ORBIT

- RANGE BIAS
- RANGE TRACKER DYNAMIC LAG
- IONOSPHERIC REFRACTION
- TRANSPONDER DELAY VARIATIONS WITH SIGNAL STRENGTH

II. SYSTEMATIC ERRORS IN THE COHERENT SIGNAL PROCESSOR

- MEASUREMENT BIAS
- SERVO LAG
- IONOSPHERIC REFRACTION
- RELATIVE TIMING ERROR

B. COMMON ERRORS LARGELY ACCOMMODATED BY THE ORBIT

- TROPOSPHERIC REFRACTION CORRECTION ERROR
- ABSOLUTE TIMING ERROR
- STATION POSITION ERROR

Category I are orbit errors caused by systematic errors in the orbit-determining ranges but not present in the integrated range data.

Category II are data errors in the CSP integrated ranges not corresponding to errors in the DIRAM ranges. Ionospheric refraction appears in both categories since it has equal but opposite effect on the group-measurement DIRAM ranges and the phase-measurement integrated Doppler ranges.

2.4 ERROR ANALYSES

CSP integrated range error analyses were undertaken for three distinct sources:

- radar systematic errors,
- computational errors: integrator error,
- uncorrected propagation effects: ionospheric refraction, tropospheric refraction correction error.

These analyses were conducted both deductively through model fitting to actual residuals and inductively using the ORAN program (4) to simulate the effects of unmodelled errors in a Bayesian Least Squares orbital solution.

2.4.1 Integrated Range Error Model

After extensive investigation, the most reasonable form for modelable error in the residuals of the integrated range data about the orbit determined by the conventional data was found to be:

$$\Delta R_i = a_o + a_1 \dot{R}_i + a_2 (t_i - t_o) + a_3 \ddot{R}_i$$

where

$\Delta\dot{R}_i$ = ith integrated range residual

a_o = offset or bias; error in the constant of integration

a_1 = relative timing error between the CSP and DIRAM systems

a_2 = range rate measurement bias in the CSP system

a_3 = 1st order lag coefficient; $\frac{1}{K_a}$; see Appendix A

$\dot{R}_i$ = range rate at ith point

$\ddot{R}_i$ = range acceleration at ith point

$(t_i - t_o)$ = elapsed "integrator time" at ith point.

Each of the four error terms represent systematic errors known to exist and quantitatively modelable. This model was fit in a batch least squares sense (Appendix B) to integrated range residuals generated in the orbit determination program GEODYN.

2.4.2 Integrator Error

The integrator for CSP ranges is a simple trapezoid rule formulation shown in Figure 2-2. It takes its name from the fact that the area of the shaded rectangle is the area of the trapezoid $(t_{i-1}, \dot{R}_{i-1}, \dot{R}_i, t_i)$. Aside from its ease in implementation, this integrator has the following characteristics:

- It is precisely accurate if the integrand is linear between adjacent sample points; thus its first order error is a function of the second derivative of the integrand. Since the second derivative of range rate ($\dddot{R}$ or "jerk") typically does not exceed .30 m/sec^3 and the integrator is exercised at the 10 pps radar sample rate (step size h = .1 sec) the local error written (5) as

$$-\frac{1}{12}\, h^3 f''(\epsilon)$$

is not expected to exceed .0025 cm. and the global error

$$-\frac{t_i - t_o}{12}\, h^2 f''(\epsilon)$$

should not exceed 15 cm., assuming that the maximum $\dddot{R}$ value prevails throughout the pass.

- It does not require equally spaced data points; it can integrate over editted points and, moreover, can be used on the series of unequally spaced (transit-time corrected) measurements generated by the radar.

It is essential to the integration process that the sample times be corrected for propagation delay (transit time) effects before the intersample Δt is computed; this intersample period is not constant as the propagation delay changes with range. Accordingly an integrator able to function with unequally spaced data is a necessity, unless a measurement interpolation scheme is implemented. The following clarifies the necessity of this correction.

The numerical integrator functions upon an ordered set of $(t_i, \dot{R}_i)$ values as sampled by the radar. The measurement times are at even .1 sec intervals of radar (ground received) time. If we assume that these measurements are "instantaneous" then we must alter the time associated with each measurement to its true effective time at the satellite,

$$T_i = t_i - \frac{R_i}{C}$$

where

T_i = true effective time of ith measurement

t_i = ground time of ith measurement

R_i = range at ith measurement

Whether the times associated with the measurements are altered before the integration process (while associated with a rate measurement) or after the integration process (while associated with a range measurement) is irrelevant in principle since the integral of ground-received rate data is ground-received range data, and conversely the integral of satellite-timed rate data is satellite-timed range data. This theoretical indifference to transit time considerations rests upon the notion of perfect theoretical integration. In fact the numerical integrator we use makes finite approximations of area at each step and to do so accurately must have a bin width (ΔT) equally as accurate as the bin height ($\dot{R}$). Even so, it too is indifferent to a time bias, i.e., it calculates

$$\Delta t = t_i - t_{i-1}$$

and if all times are in error by a bias

$$t_i = T_i + \epsilon$$

we still have

$$\Delta t = t_i - t_{i-1}$$

$$= (T_i + \epsilon) - (T_{i-1} + \epsilon)$$

$$= \Delta T$$

The fundamental point here is that transit time is not a bias and does not fit this model. Even for two points .1 sec apart, the true "width" of the "bins" differs significantly. Mathematically,

$$T_i = t_i - \frac{R_i}{C}$$

$$T_{i-1} = t_{i-1} - \frac{R_{i-1}}{C}$$

$$\Delta T = T_i - T_{i-1} = (t_i - t_{i-1}) - \frac{R_i - R_{i-1}}{C}$$

which simply says that our bin widths differ from .1 sec by an amount proportional to the change in range over .1 sec. This is clearly a range rate dependent error; indeed, we can write

$$\Delta T = (t_i - t_{i-1}) - \frac{(R_i - R_{i-1})\ \frac{(t_i - t_{i-1})}{(t_i - t_{i-1})}}{C}$$

$$\Delta T = (t_i - t_{i-1}) \left(1 - \frac{\left(\frac{R_i - R_{i-1}}{t_i - t_{i-1}} \right)}{C} \right)$$

$$\Delta T \approx (t_i - t_{i-1}) \left(1 - \frac{\dot{R}_i}{C} \right)$$

$$\text{as } (t_i - t_{i-1}) \longrightarrow 0$$

The magnitude of this error is clearly illustrated in Figure 2-8, a typical GEOS-3 range rate plot with two additional scales, transit time rate, and actual intersample ΔT at the 10 pps ground received sampling rate.

Returning to the integrator formulation,

$$R_i = R_{i-1} + \frac{\dot{R}_i + \dot{R}_{i-1}}{2} \Delta T$$

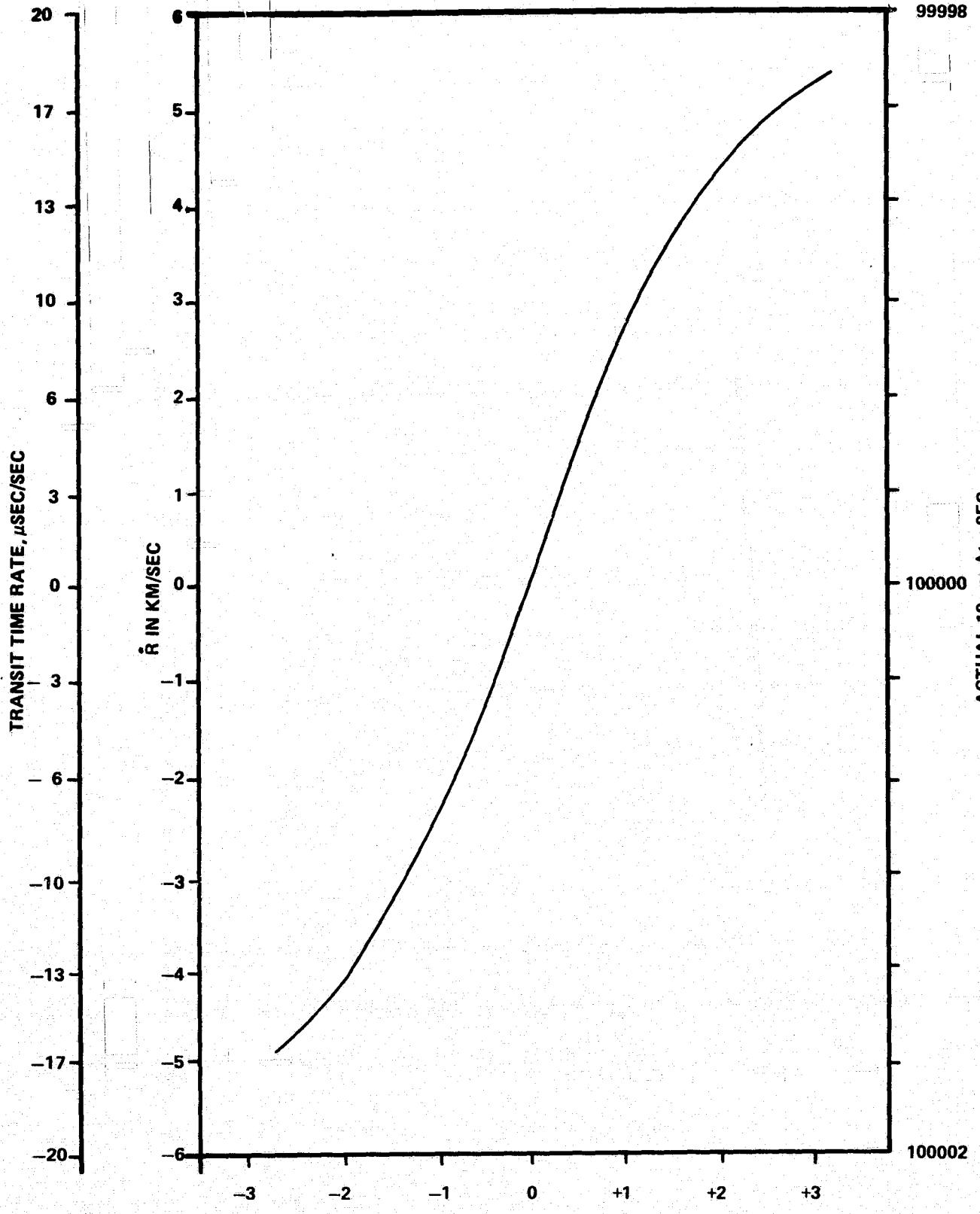

FIGURE 2–8. TYPICAL GEOS–3 RANGE AND TRANSIT TIME RATES

we find that an error in ΔT of $\frac{\dot{R}\Delta t}{C}$ produces a local error in the integrated range increment of

$$\epsilon = \left(\frac{\dot{R}_i \Delta t}{C}\right) \left(\frac{\dot{R}_i + \dot{R}_{i-1}}{2}\right)$$

$$\epsilon \approx \frac{\dot{R}_i^2 \Delta t}{C}$$

Figure 2-7 shows the local error $\frac{\dot{R}_i^2 \Delta t}{C}$ for a 55^o pass. The expected global error for the pass is the sum ($\approx$ integral) of these local errors. Figure 2-10 shows the actual residual plot of Rev 4547 integrated with a constant .05 sec (20 pps) step size, not corrected for transit time. This error is independent of stepsize, since doubling the stepsize results in half as many steps, each with twice as much error.

2.4.3 Propagation Effects

2.4.3.1 Tropospheric Refraction Error

As previously stated in Section 2.3, tropospheric refraction effects should not produce significant errors in the integrated range residuals as processed for this study. Ranges are corrected for tropospheric effects with a model (6) incorporating local meteorological data and good to approximately 2-3%. The residual refraction error is a smooth function, primarily of elevation, which is almost entirely accommodated by the reference orbit fit to the conventional range data at elevation angles above 15^o. Since the residual error in the integrated ranges is identical, it is not observable in residuals about the reference orbit.

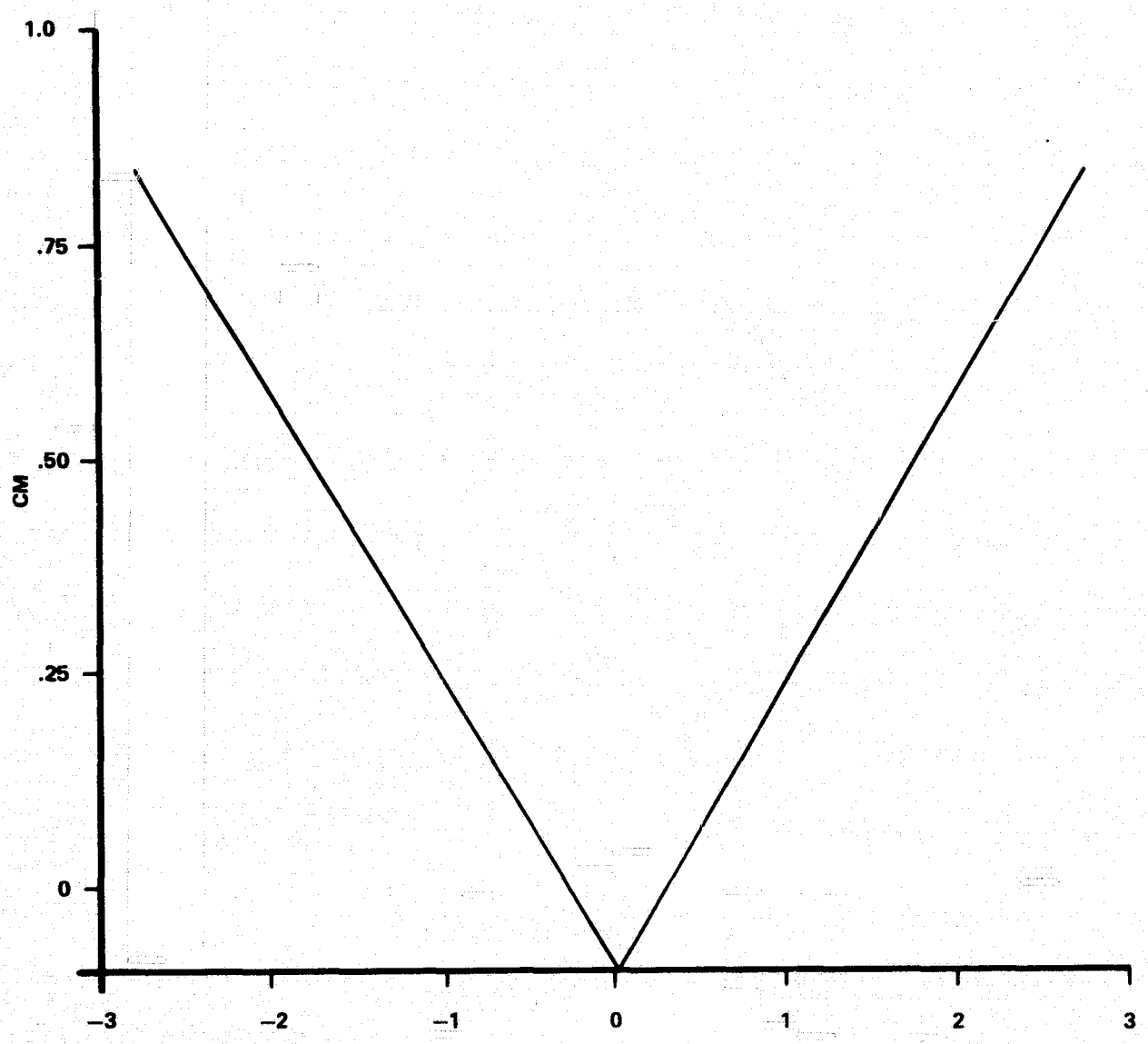

FIGURE 2–9. APPROXIMATE LOCAL INTEGRATION ERROR, 55° PASS, FROM NEGLECT OF TRANSIT TIME

FIGURE 2–10. GEOS–3 INTEGRATED RANGE RESIDUALS
REV 4547 WALLOPS AN/FPQ–6
TRANSIT TIME CORRECTED AFTER INTEGRATION

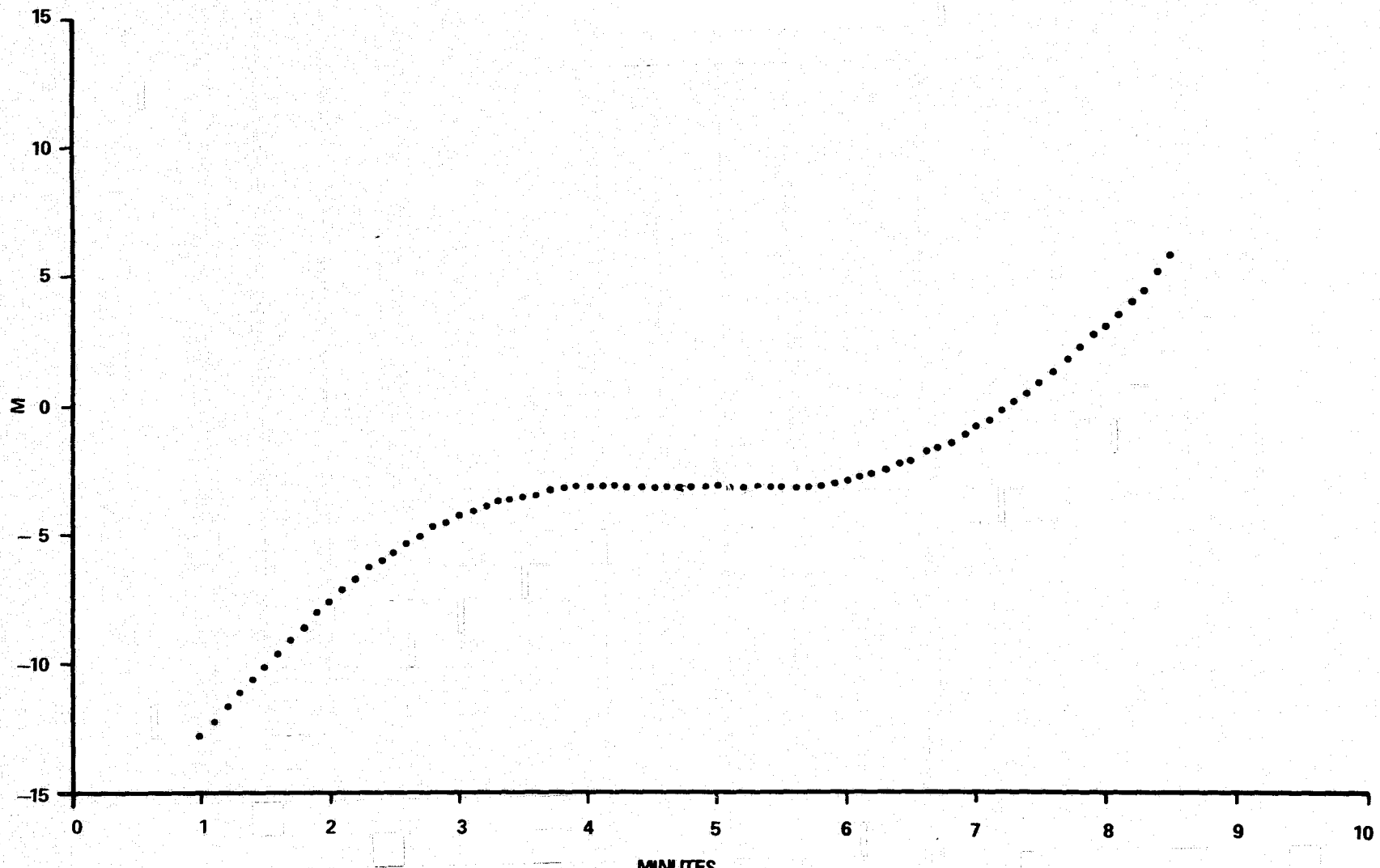

2.4.3.2 Ionospheric Refraction Error

Accurate quantitative modeling of ionospheric refraction error effects is extremely difficult and can require reasonably good estimates of solar flux values for the time of the data in question. In general, C-Band tracking data has not been routinely corrected for ionospheric effects by any investigators known to us. However, since the effect of the ionosphere will be equal but opposite on the two ranging data set types discussed here, and because of the very low noise of the integrated range residuals where the effects were expected to be visible, some quantitative modeling was attempted using a modified version of the BENT ionospheric model in the ORAN program. The results are discussed in Section 3.0.

2.4.4 Range Bias Effects

Analysis of the pass presented in detail in the following section, Rev 9799 as tracked by the Wallops AN/FPQ-6, benefitted from a reliable estimate of the total range bias in the DIRAM ranges used to compute the reference orbit. This bias was recovered from a two-consecutive - revolution solution making use of the tracking data available from the same radar for Rev 9800. During the course of the study, however, many passes were examined which either had no such estimate or which were initially preprocessed incorrectly in such a manner as to introduce a large bias. In each of these cases a distinct "M" or "W" shape was observed in the integrated range residuals and where the bias was extreme (such as neglect of transponder delay, $\approx$ 380m) in the ordinary DIRAM range residuals.

An ORAN analysis determined that this shape is characteristic of the effect of a range bias on a single-station single pass orbital solution. The sense of the pattern (M or W) is determined by the sign of the bias. It is best explained as the geometrical resolution of a constant bias in slant range into varying proportions of along-track and radial error, as the station-satellite geometry changes during the pass. The pattern is produced by the nature of a least-squares orbital solution and its attempt to find the one trajectory that best accomodates this changing error. Figure 2-11 shows the effect of a 10m bias as predicted by the ORAN program for both a low and high elevation pass. As might be expected, the effect is most pronounced in high elevation passes.

In fact this phenomenon had been noted before in cases where an extremely large bias had been introduced into conventional range data through error or oversight. Its significance was minimal because of the magnitude of the effect: as the figure shows, a 10m bias in a high elevation pass produces only a 1m effect; in prior analysis of C-Band ranging data with an RMS noise level of 1m or more such an effect was largely unresolvable. However, the availability of extremely low noise range measurement from a C-Band radar may significantly

FIGURE 2–11.

EFFECT OF 10m RANGE BIAS ON RANGE RESIDUALS

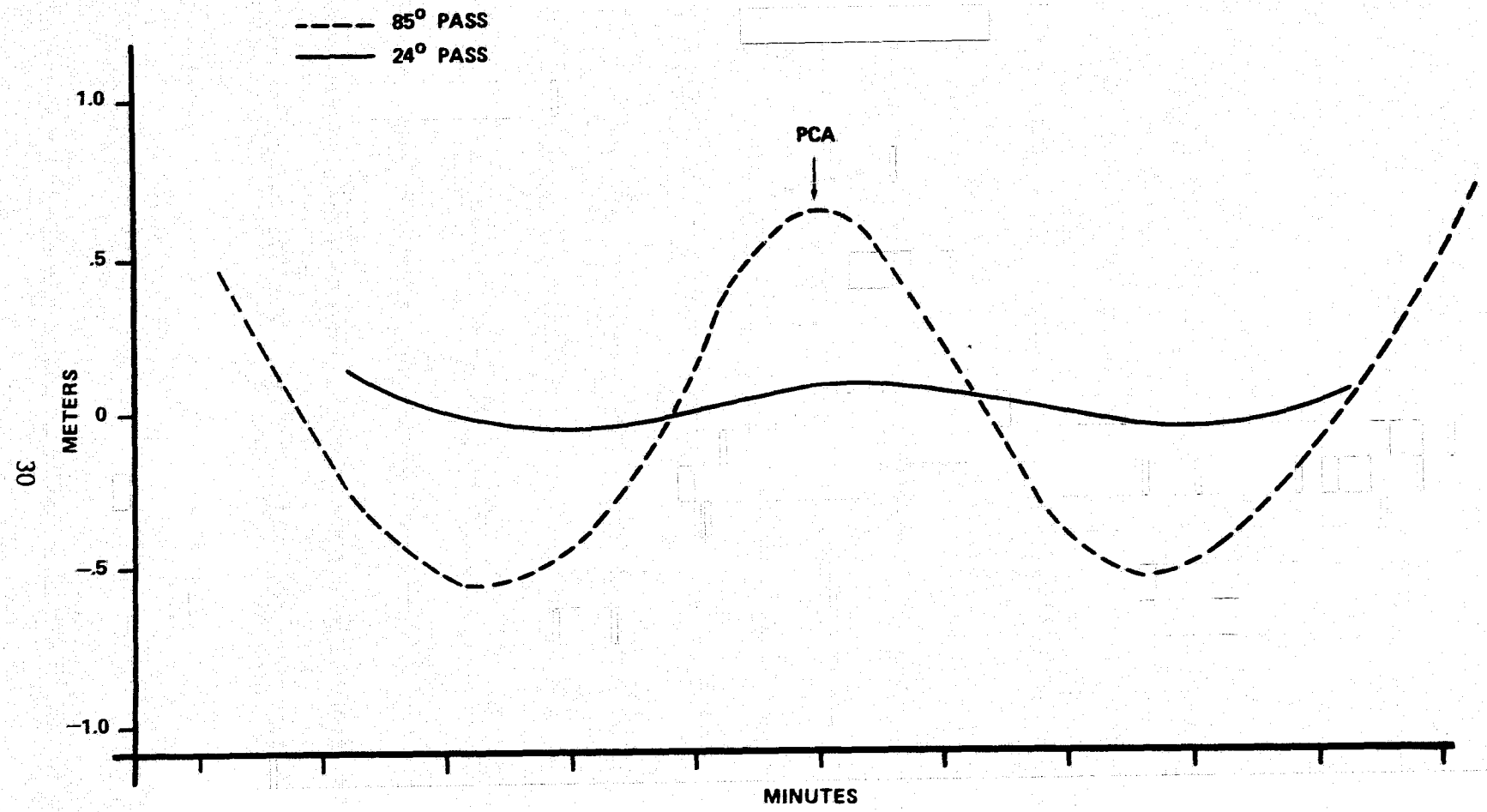

increase the importance of this phenomenon. Scaling from the figure, a 1m bias produces an "M" or "W" shape on the order of 10 cm at high elevations; this is well below the potential resolution of the integrated Doppler range data. With the availability of accurate radar error parameter values and good quantitative estimates of ionospheric propagation effects, the possibility of recovering range bias estimates to less than a meter from data at a single station during a single pass could significantly enhance the value of the C-Band network in geodetic studies.

SECTION 3.0
RESULTS

The results of the rather complex chain of processing, correction, error modeling, and analysis of integrated CSP ranges and the equally important reference orbit determining conventional DIRAM ranges is described sequentially for a typical data set in Section 3.1. This somewhat iterative solution is also a semi-chronological recreation of the development of the various techniques over the course of the study. Representative results from other passes are presented in Section 3.2.

Prior to any of the analyses presented here, rate data and the integrated ranges produced from it are corrected for a constant timing error relative to the conventional range data. This error was discovered and analyzed prior to the work described in this report and has been described in detail by Krabill and Dempsey (7). It is related to the update rate of the local oscillator in the CSP system. The error was determined to be correctable as a timing bias equal to one-half the update interval, usually the radar's pulse repitition interval (PRI), and has become known as the $\frac{PRI}{2}$ error. It is not discussed further in this report.

3.1 REV 9799

3.1.1 Preliminary Integrated Range Corrections

Figure 3-1 shows the results of applying the basic integrated Doppler range technique to Rev 9799 as tracked by the Wallops Island AN/FPQ-6 on March 2, 1977. No special corrections were made to the range rate data before or during the integration process other than the timing error previously discussed. The simultaneous DIRAM range data set is shown in Figure 3-2. It has been corrected for bias on the basis of pre- and post-mission ranging to a surveyed range target. Both data sets have been corrected for transit time and tropospheric refraction effects. The DIRAM ranges were reduced to the 10 per minute rate by the polynomial midpoint filter technique detailed in Section 2.2.1.

FIGURE 3–1. UNCORRECTED GEOS–3 CSP INTEGRATED RANGE RESIDUALS
REV 9799 WALLOPS AN/FPQ–6
RMS 4.5 m

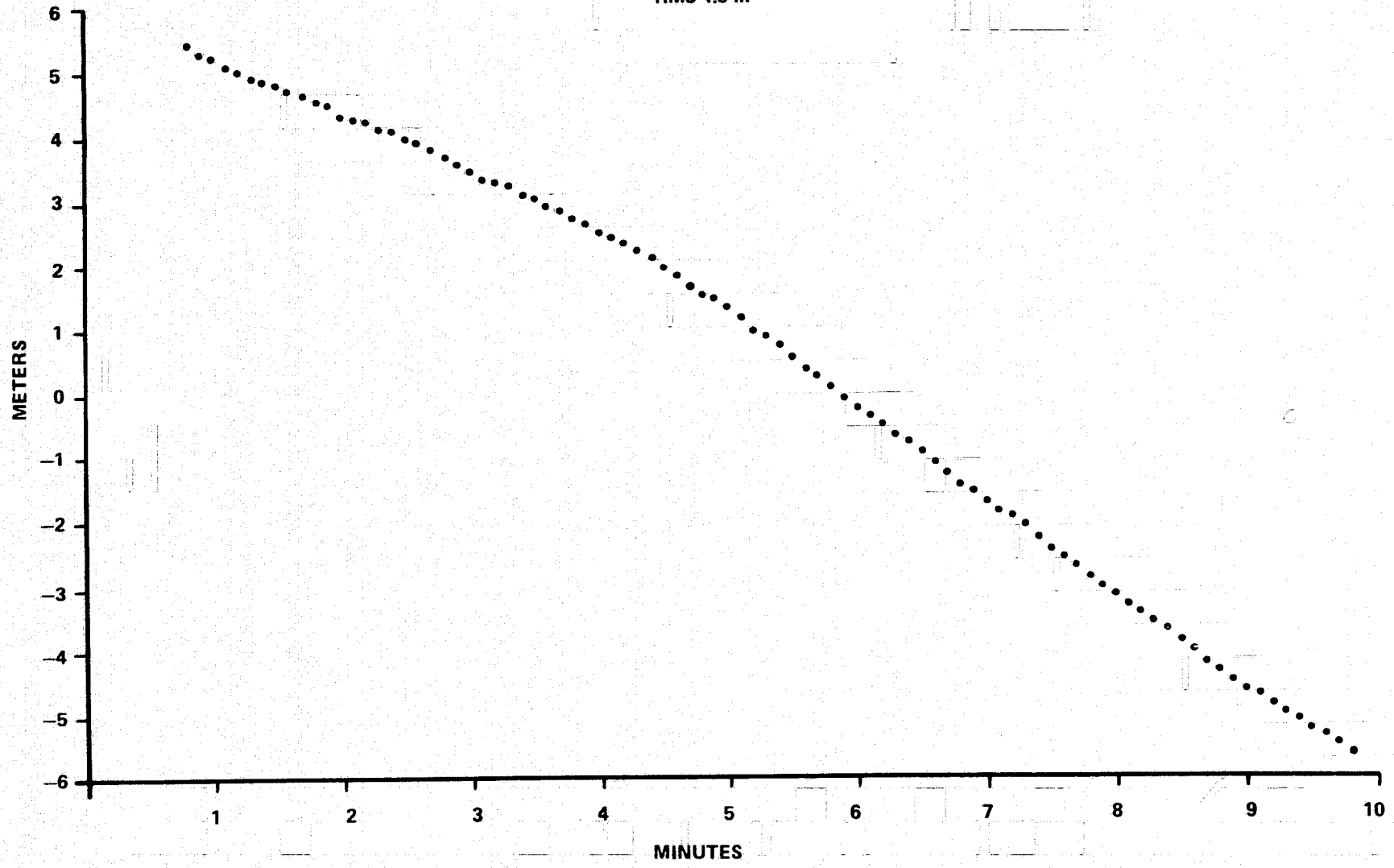

FIGURE 3-2.
REV 9799 RANGE RESIDUALS

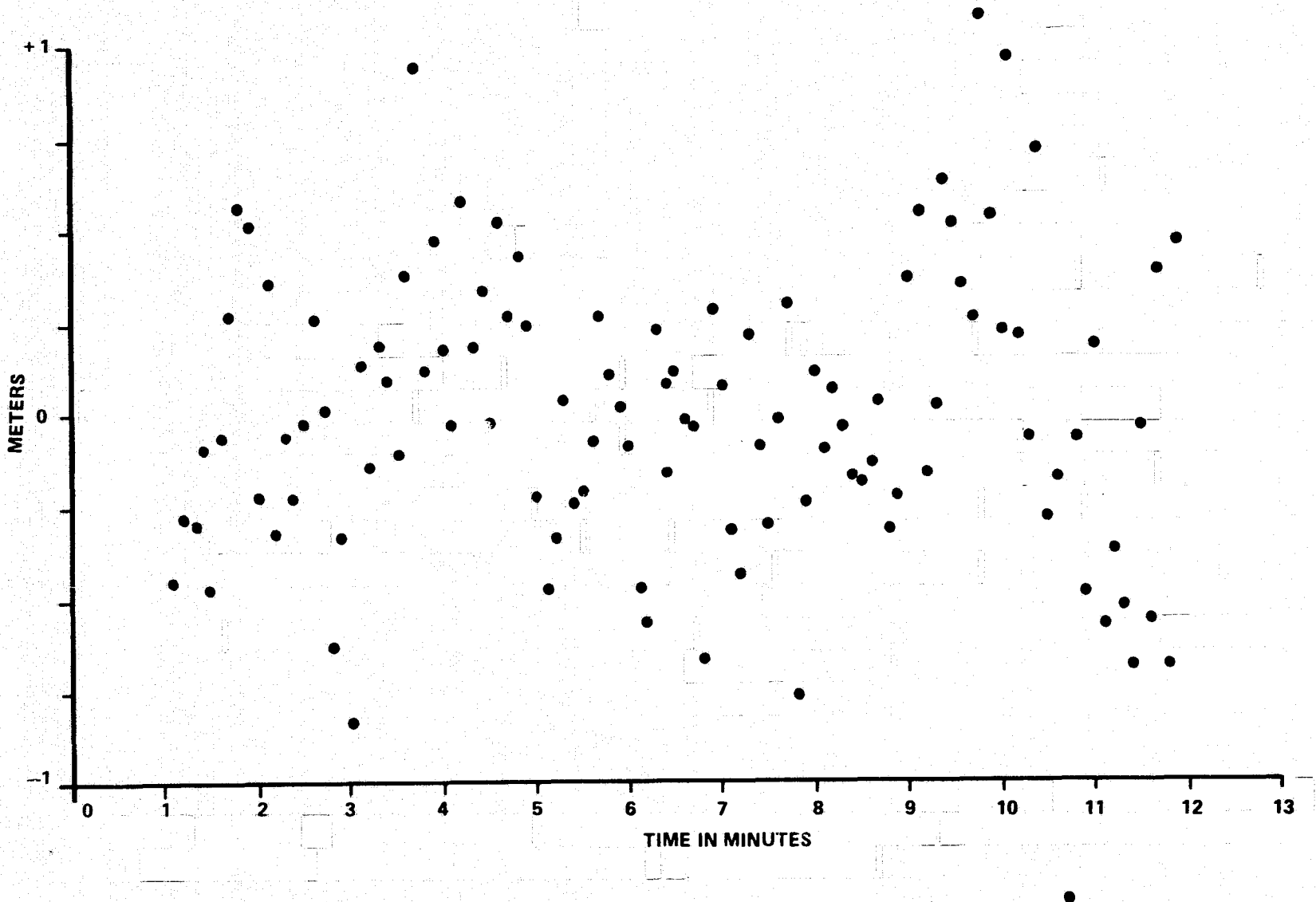

The principle trend in the uncorrected integrated range data is the monotonic decrease consistent with a constant bias ($\approx$ 2 cm/sec in this case) in the range rate measurement. It illustrates the sensitivity of the integrated ranges to systematic error and their ability to magnify such effects. The bias is a known error stemming from a discriminator curve offset. A hardware calibration technique was developed to estimate this bias, based on driving the CSP system up one spectral line and down one spectral line during pre- and post-mission calibration periods. This data is recorded on tape and can be reduced to yield the true CSP zero, which is essentially the mean of the two equal in magnitude but oppositely signed rate measurements. Figure 3-3 shows the data after this calibration correction to the range rate measurements is taken into account during the integration process.

The residual effects were thought to be some combination of:

- Servo dynamic lag
- Ionospheric refraction effects
- DIRAM range bias effect on the reference orbit
- Residual timing bias in the CSP system (after PRI/2 correction).

However, attempts to recover (Appendix B) consistant estimates of error model parameters (lag coefficient and timing bias) from this and other data sets proved futile. The various error sources appeared to produce highly correlated effects that were difficult to separate in a least squares recovery, i.e., the solution was weak and the estimates highly correlated. Most disturbing of all, the characteristic residual patterns seemed not to show the predicted effect of servo lag in the conventional sense. In fact, the residual patterns and the lag coefficient estimates recovered from them tended to be the reverse of what was expected, i.e., the servo appeared to "lead." This observation initiated a search for a systematic error source whose signature might be nearly opposite to that expected from CSP servo lag effects. This error source was ultimately identified in the DIRAM ranges defining the reference orbit.

FIGURE 3–3. GEOS–3 CSP INTEGRATED RANGE RESIDUALS
REV 9799 WALLOPS AN/FPQ–6
CSP RANGE RATES CORRECTED FOR BIAS BEFORE INTEGRATION

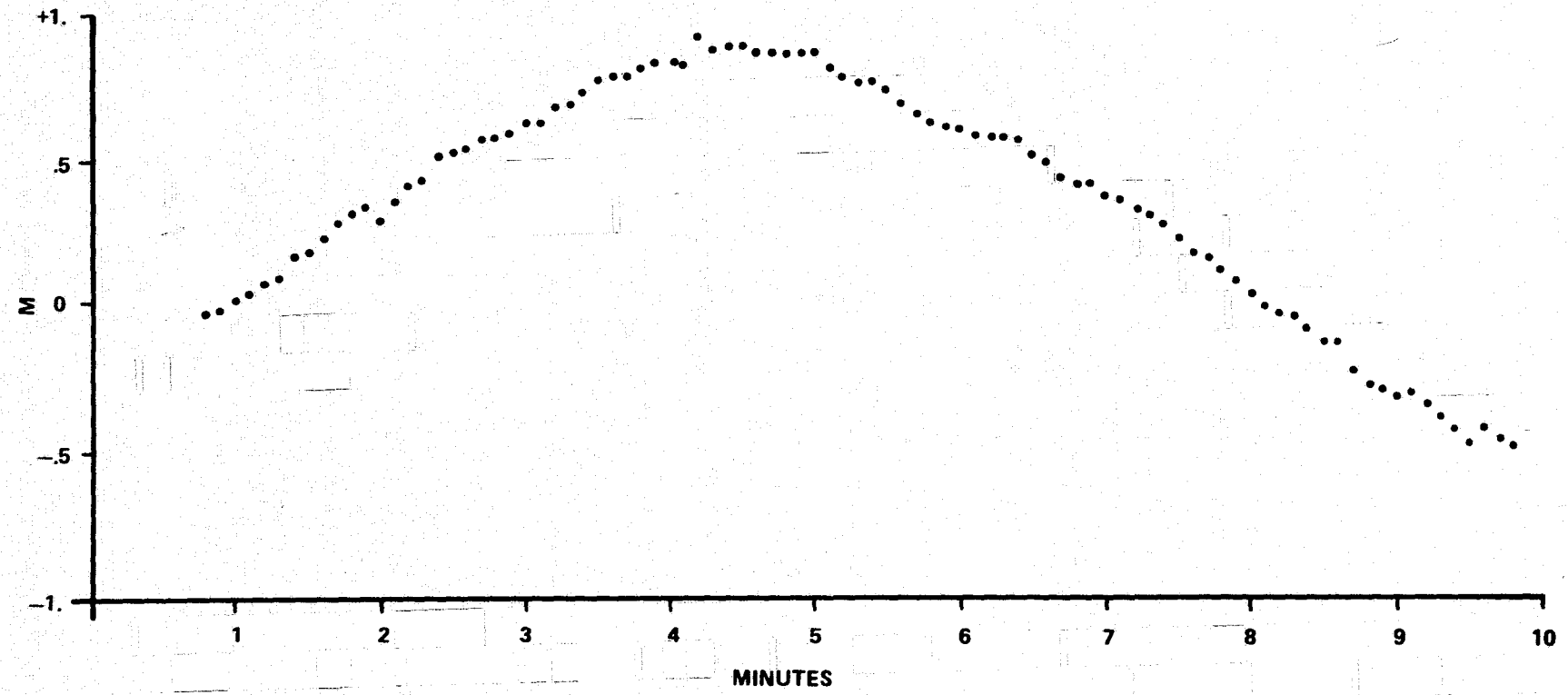

3.1.2 Beacon Delay Variation

As described in Section 2.2.2, pre-flight test data indicated that the GEOS-3 coherent beacon delay might vary significantly with signal strength in nominal operating conditions. Analysis indicated that this error effect in the DIRAM ranges, if accomodated by the reference orbit, could produce an "error" pattern in the integrated range residuals quite similar to that expected from CSP servo dynamic lag effects, but of opposite sign. Accordingly, the technique of correcting range data for beacon delay variation was developed and applied.

Figure 3-4 shows the range correction this technique produced for each of the DIRAM range measurements during the pass in question. This figure shows that, as calculated by the K-factor method previously described, the beacon delay was approximately nominal 379.48 m at PCA for this pass. To either side of PCA, the beacon delay was longer due to decreased signal strength at longer ranges; the proper compensation being a negative range increment to "shorten" the recorded ranges - in this case by as much as two meters. The step-like effect prior to PCA represents toggling of the relatively coarse radar AGC least significant bit. The large excursion after PCA is probably representative of an antenna null or lobing effect. The overall bell shape could easily be accomodated by the reference orbit fit to this single pass from a single station. The excursion, however, should have been evident in the DIRAM range residuals. Figure 3-5 shows the uncorrected DIRAM residuals and the residuals after correcting the data for beacon delay variation and fitting a new reference trajectory. The reduction of the group of "long" ranges in the area of the antenna null event is apparent.

Figure 3-6 shows the same integrated range data as Figure 3-3, displayed however as residuals about the reference orbit determined by the beacon delay variation corrected DIRAM ranges. A "bucket" shaped pattern more consistent with the expected effects of CSP servo dynamic lag is visible. Least-squares

FIGURE 3-4.
RADAR AGC
BEACON DELAY CORRECTIONS
REV 9799
WALLOPS FPQ-6

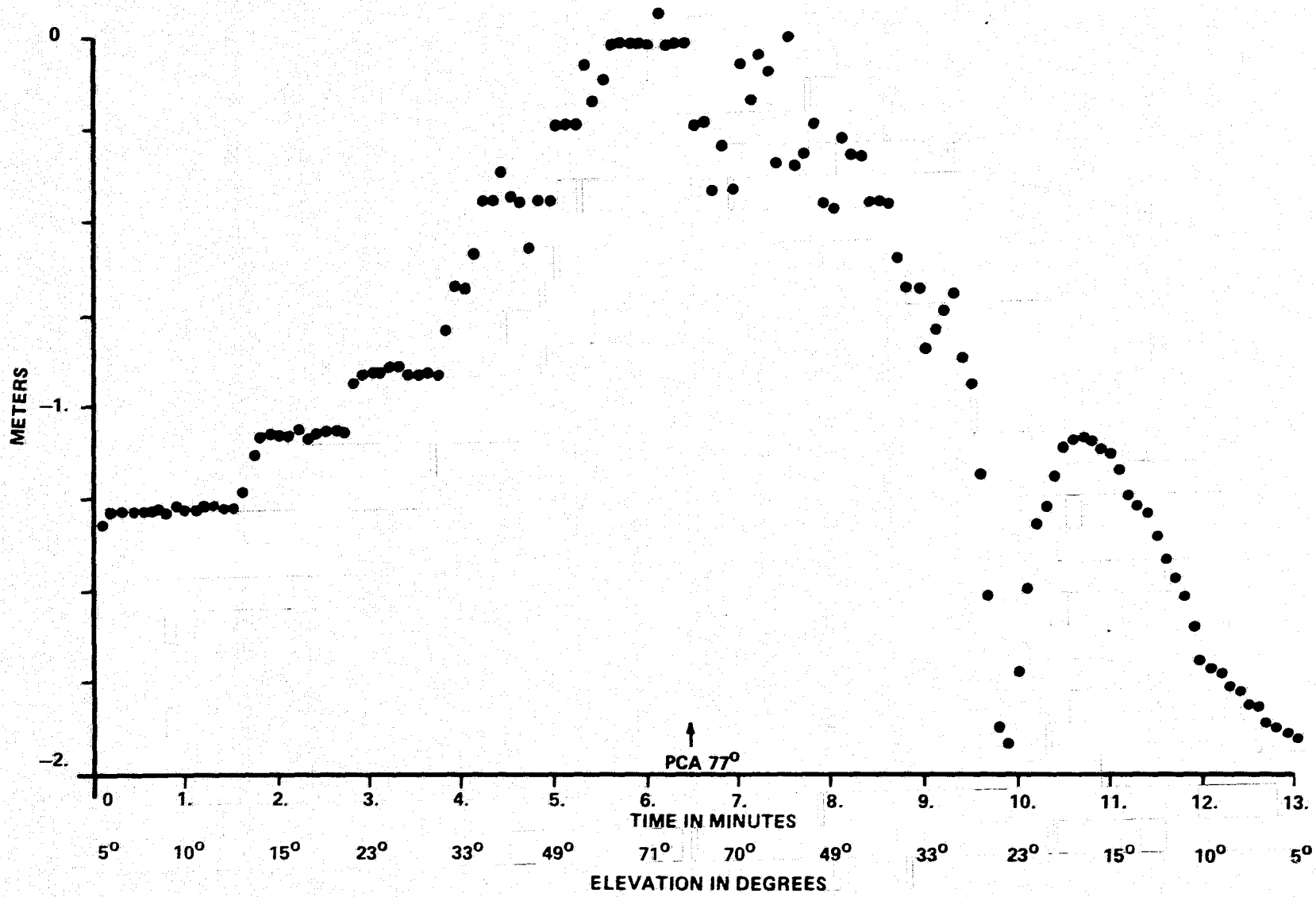

FIGURE 3-5.

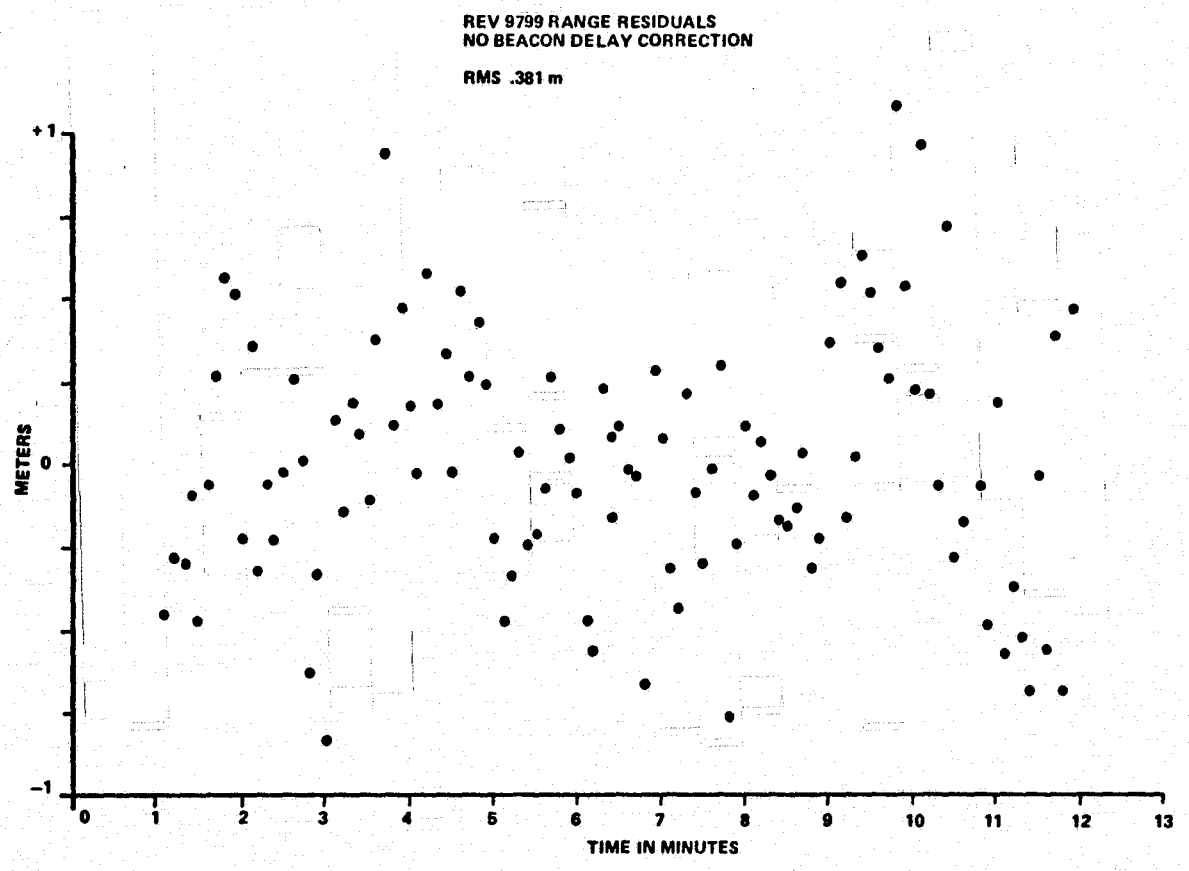

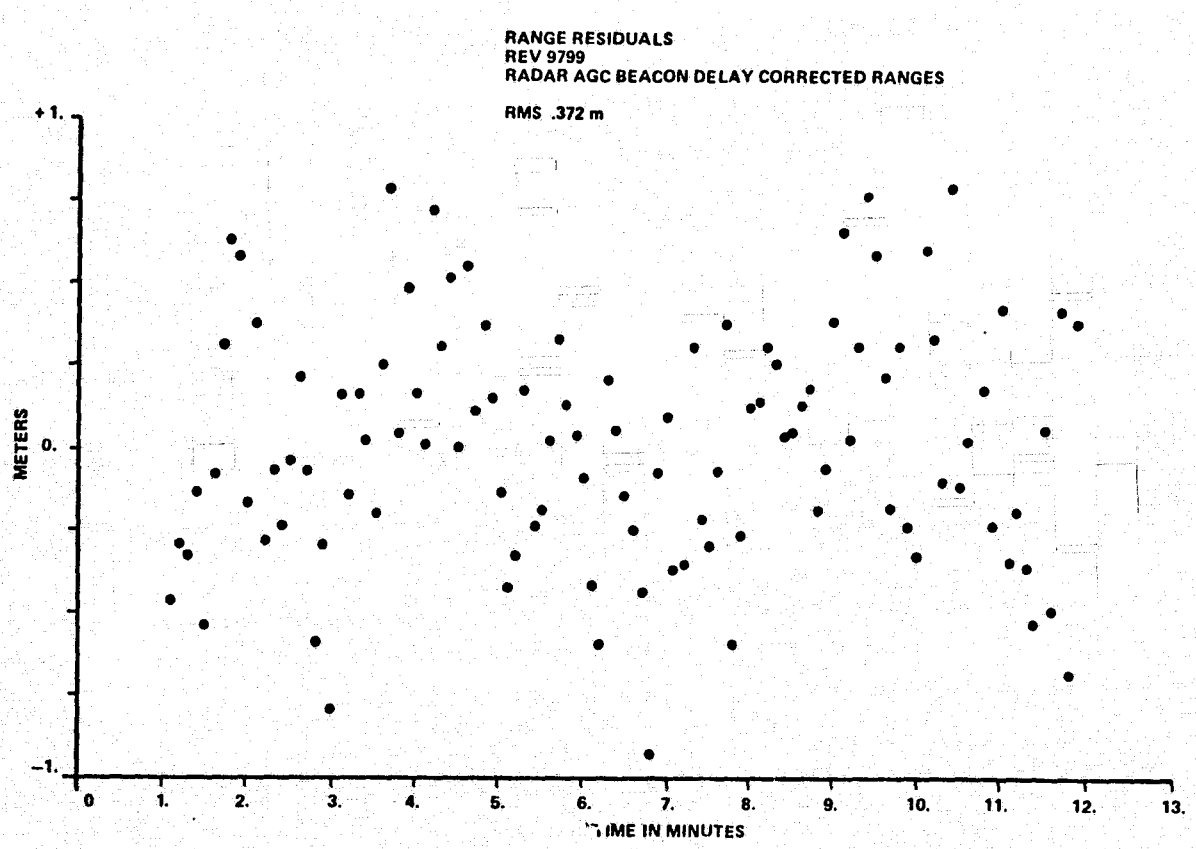

FIGURE 3–6. GEOS–3 CSP INTEGRATED RANGE RESIDUALS
REV 9799 WALLOPS AN/FPQ–6
REFERENCE ORBIT FROM DIRAM RANGES WITH BEACON DELAY VARIATION CORRECTED

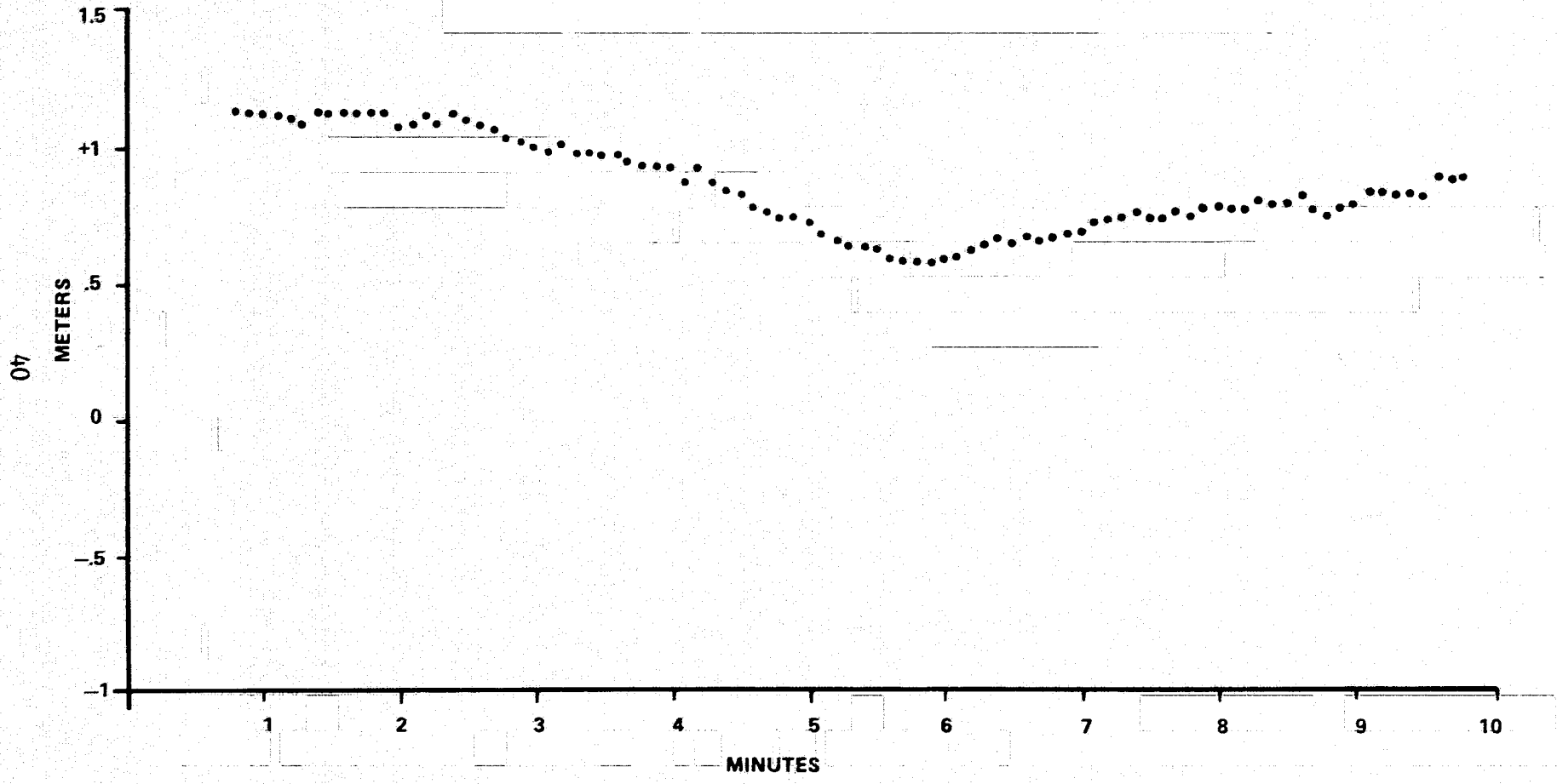

estimation of error model parameters yields the results shown in Figure 3-7. These results show considerable improvement over those that had been obtained earlier - essentially negligible residual timing and range rate bias errors, and a lag coefficient estimate K_a = 165, compared with the nominal K_a of 225 for the servo in this bandwidth. The residual data illustrates the extremely low noise (3 cm RMS in range) of this data. However, the data cannot be considered fully correct as a significant ionospheric refraction effect should still be present. We conclude that the multi-parameter error model can accomodate almost any smooth function through aliasing in one or another of its parameters. Although useful in the exploratory stages of this technique, it was concluded that consistent a priori estimates of system error parameters were necessary.

The nominal estimate of system relative timing error after the PRI/2 correction is essentially zero (7). The estimation of range rate bias with the one line up/one line down technique is thought to be quite good; however a 10% error in the estimation of a typical bias (1.5-2 cm) would significantly affect integrated range results. Similarly, the nominal servo lag coefficients K_a, are expected to be accurate $\pm$ 15%, but this also is too great a range for consistant data reduction of the integrated ranges. For example, Figure 3-8 shows the results for the subject pass when corrected, a priori, for

- Residual timing bias: 0.
- Range rate bias: one line up - one line down estimate of -2.04 cm/sec.
- Servo lag: K_a = 225.

This can be compared to Figure 3-9, the predicted effects of ionospheric refraction as observed in the corrected integrated range residuals about the reference orbit. The disagreement between these two figures could be explained almost entirely on the basis of uncertainty in the error model coefficients and difficulty in obtaining accurate quantitative estimates of ionospheric propagation effects.

FIGURE 3-7.

REV 9799

CSP INTEGRATED RANGE RESIDUALS

$\Delta t = -38\ \mu sec$

$\Delta \dot{R} = .04$ cm/sec

$K_a = 165$

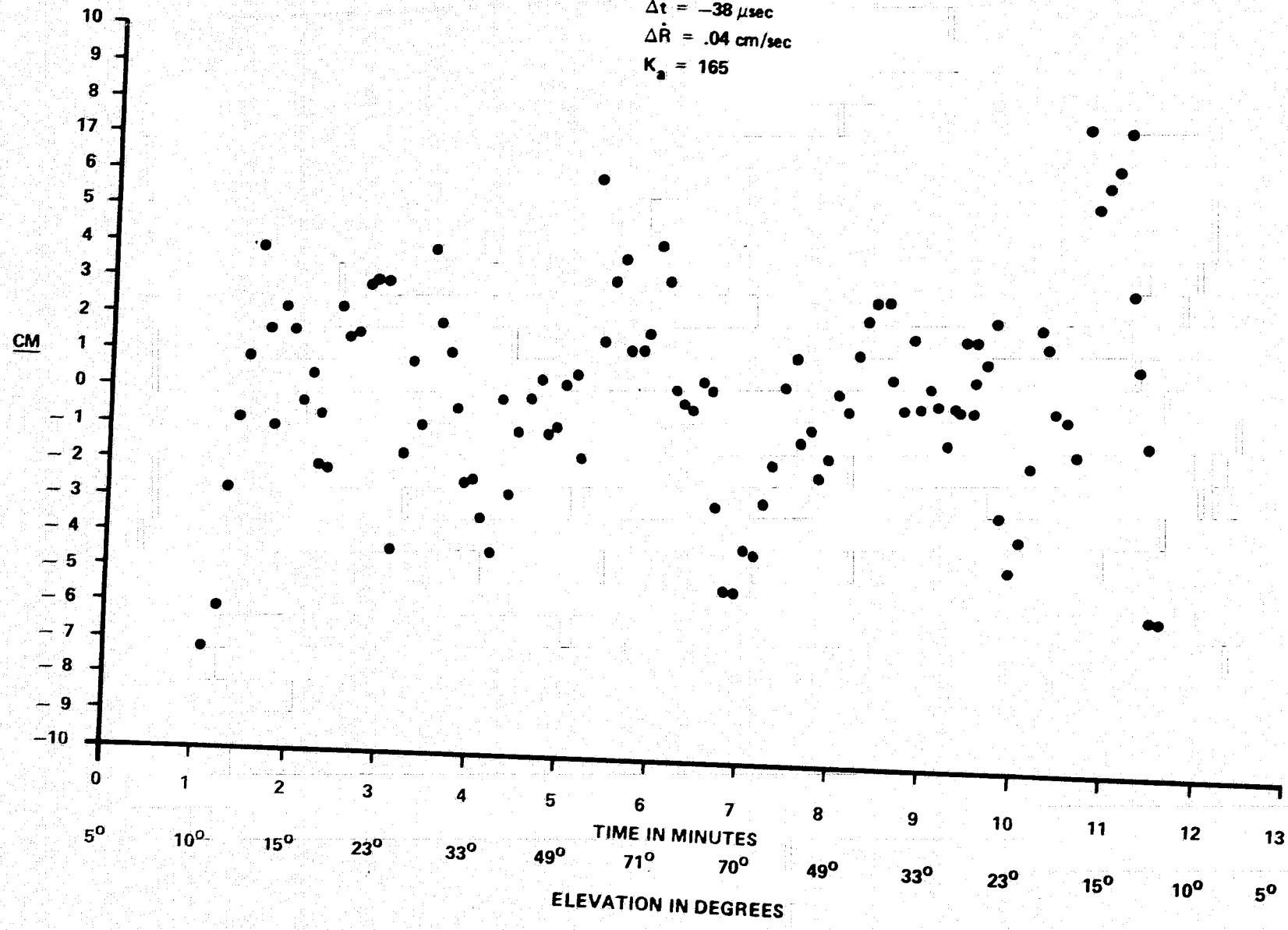

FIGURE 3-8.

REV 9799

CSP INTEGRATED RANGES ABOUT DIRAM RANGE ORBIT

A PRIORI CORRECTIONS

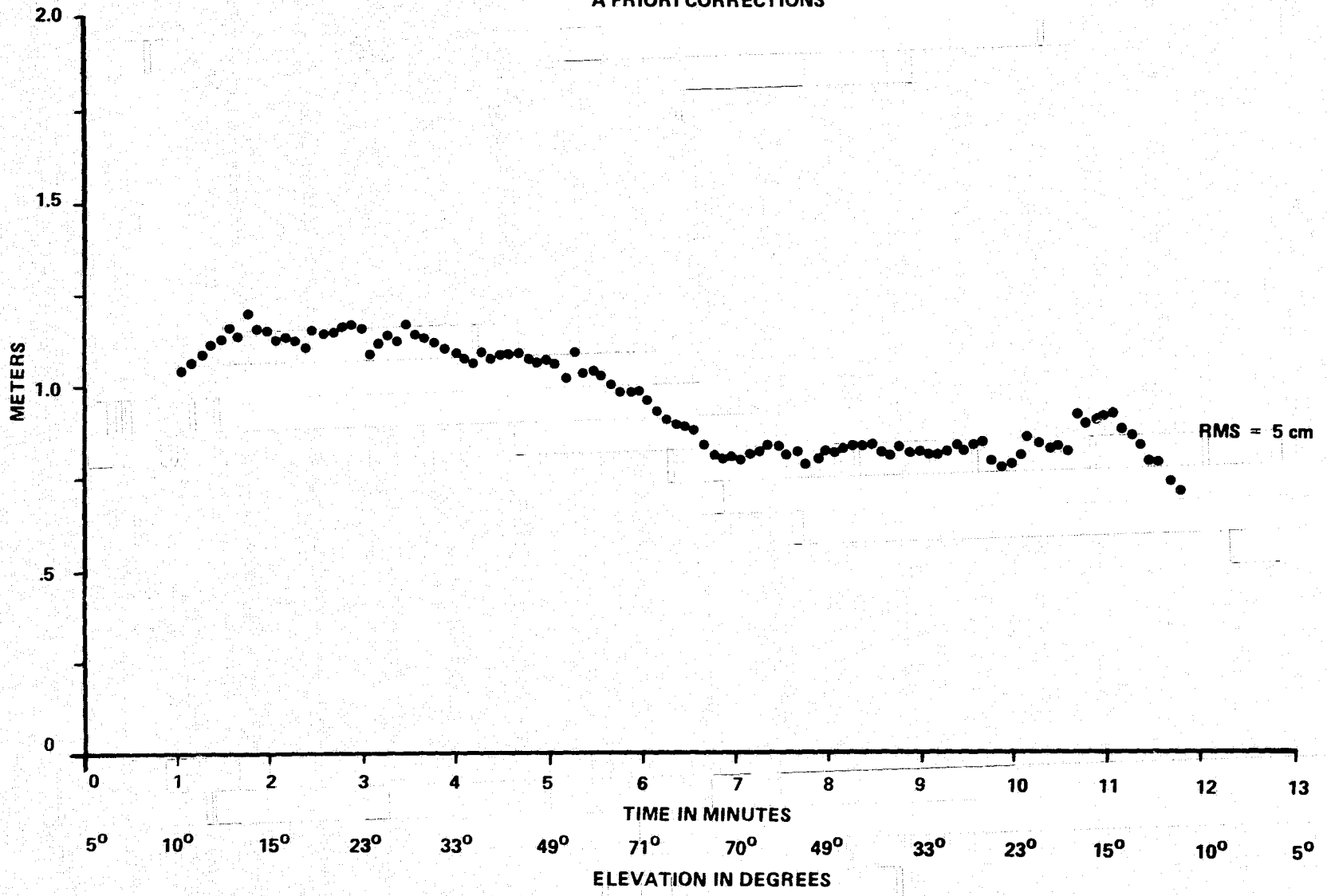

FIGURE 3-9.

ORAN PREDICTED IONOSPHERIC EFFECTS

REV 9799

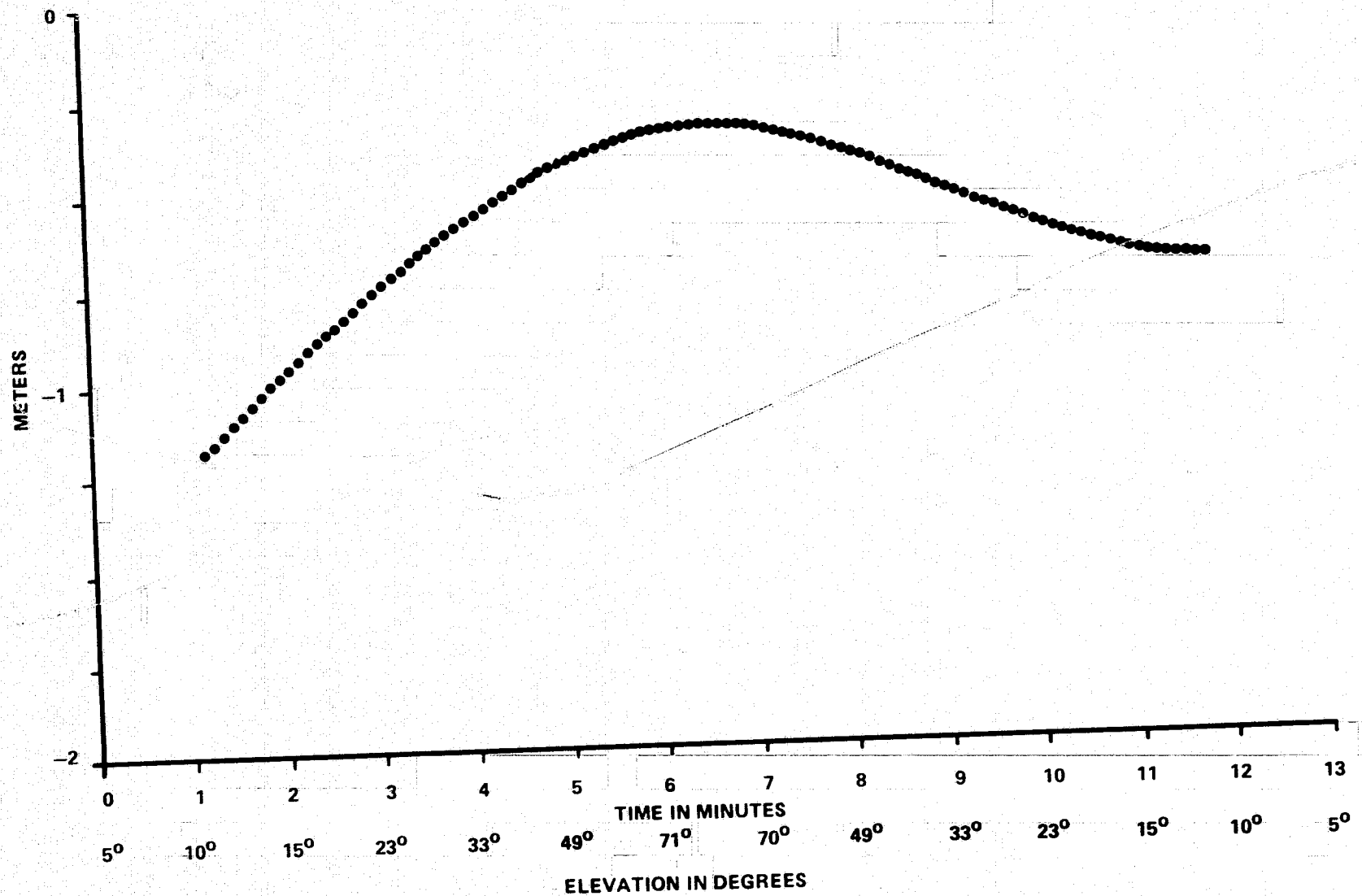

3.2 OTHER CASES

Several other typical results are shown in Figures 3-10 through 3-12.

Figure 3-10 shows the integrated range residuals for Rev 202 after the least squares solution for the radar error parameters. Again, the values recovered are in reasonably good agreement with the nominal estimates of K_a = 27, $\dot{R}$ bias after calibration = 0., relative timing error after PRI/2 correction = 0. However, the effects of ionospheric refraction have been largely absorbed by these estimates. In particular, the relative timing error estimate of almost half a millisecond is much too large and probably due in large part to this effect. The remaining residual pattern shows a "W" shape consistent with a small bias in the DIRAM ranges used to compute the reference trajectory. The small tails at the extremes of the "W" are thought to be the effects of tropospheric refraction model errors which are not totally accommodated by the reference orbit at very low elevation angles. The effect here is limited to data between 10^{o} and 15^{o} elevation.

Figure 3-11 shows the integrated range residuals for the next consecutive revolution, Rev 203, corrected a priori for the nominal error parameters as indicated in the figure. The remaining pattern is characteristic of predicted effects of the ionosphere, which are not always symmetric due to spacecraft motion toward or away from the sun. Deviation of the pattern from the actual effects of the ionosphere is attributed to error in the a priori estimates of radar error parameters used to correct the data.

Figure 3-12 shows the integrated range residuals from Rev 11704, once again after correction by least-squares recovery of error parameters. In this case the effect of the ionosphere apparently served to largely cancel servo lag effects; the recovered K_a was essentially infinite indicating no lag, while the range rate timing and measurement bias estimates were more reasonable.

FIGURE 3–10. REV 202 INTEGRATED RANGE RESIDUALS

SOLVED PARAMETERS K_a = 32

$\dot{R}$ BIAS = 1 mm/sec

Δt = 468 μsec

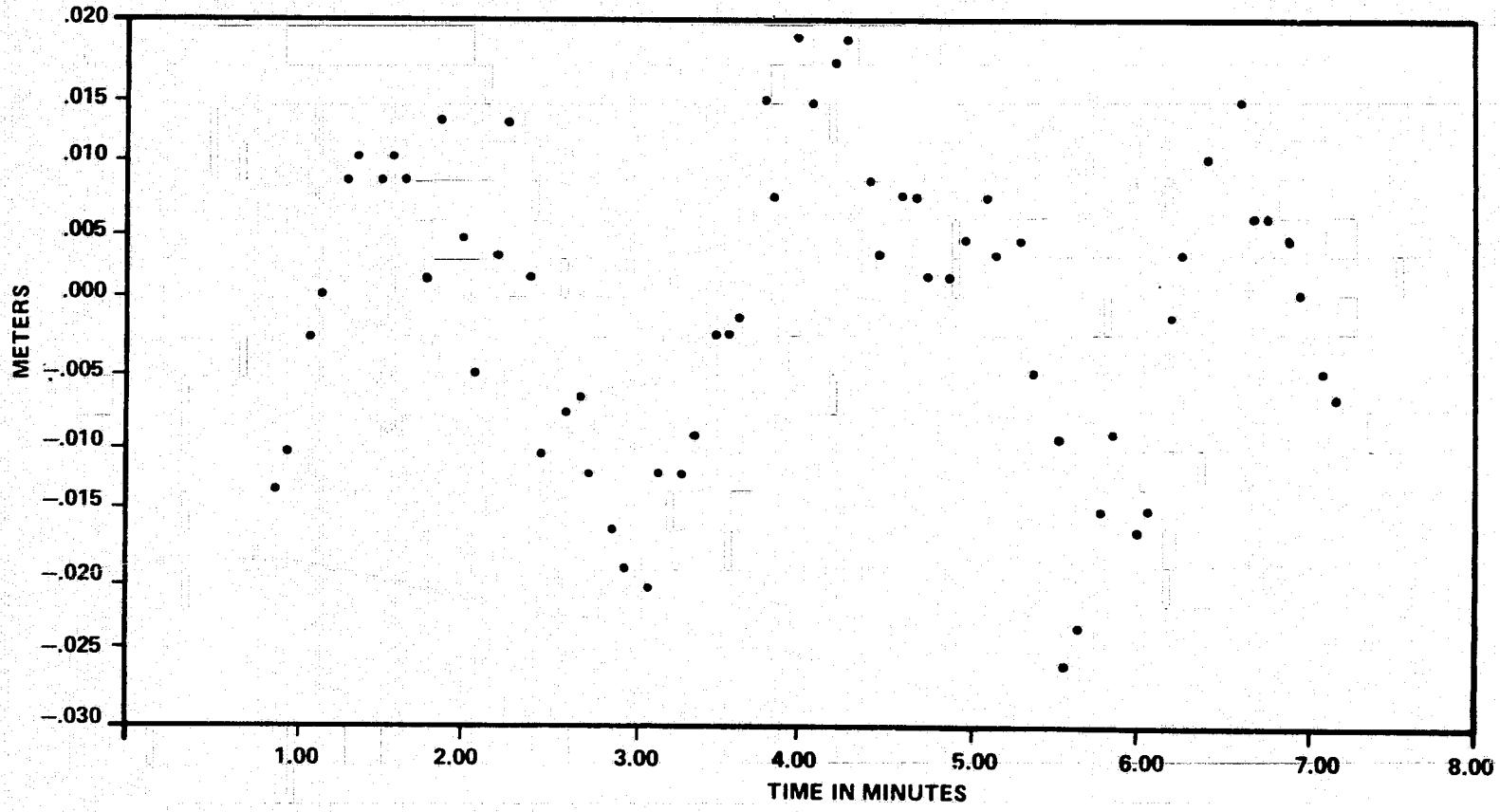

FIGURE 3–11. REV 203 INTEGRATED RANGE RESIDUALS

A PRIORI PARAMETERS $K_a = 27$

$\dot{R}$ BIAS = 0.

$\Delta t = 0.$

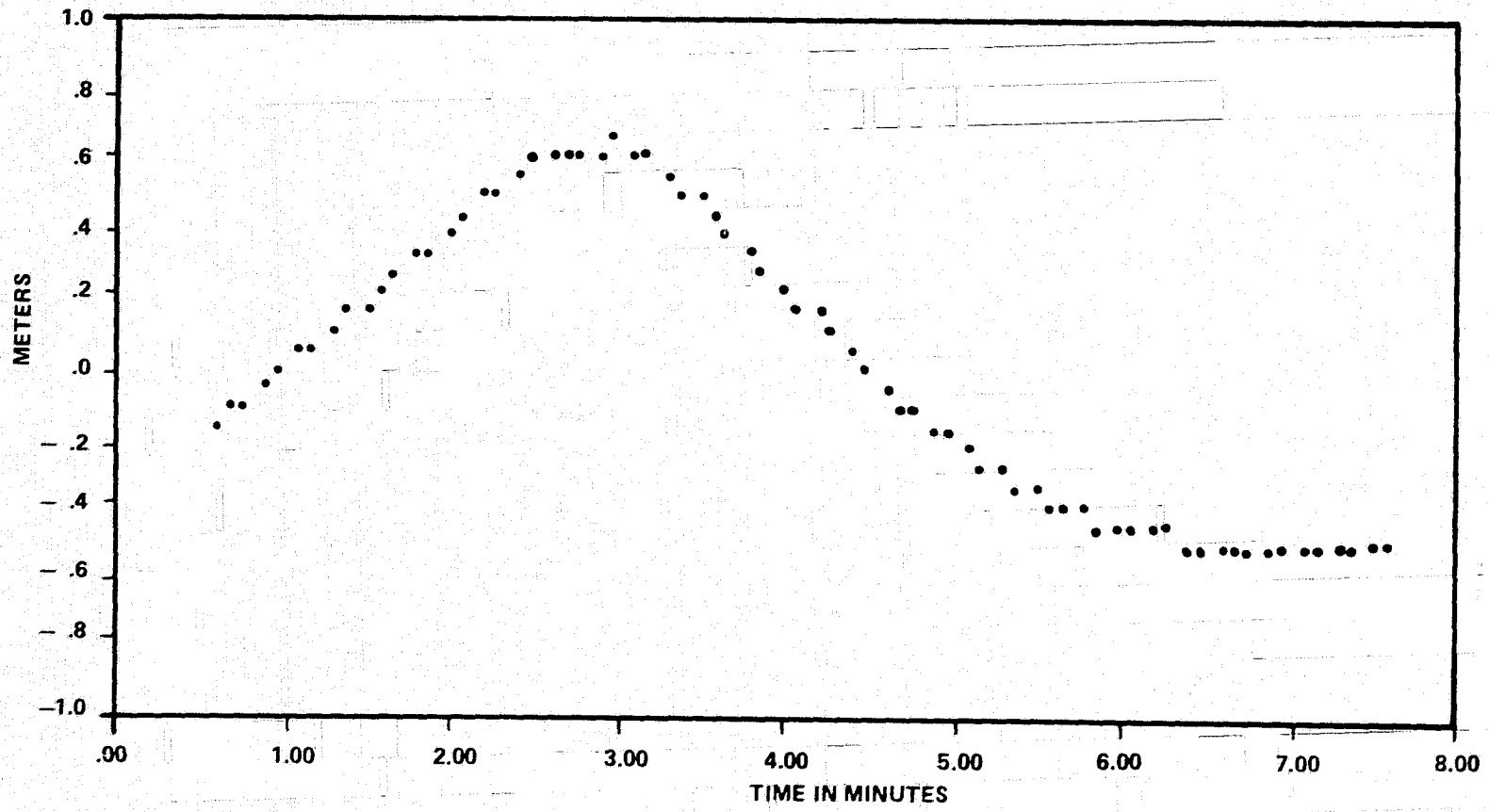

FIGURE 3–12. REV 11704 INTEGRATED RANGE RESIDUALS

SOLVED PARAMETERS $K_a = \infty$ (no lag)

$\dot{R}$ BIAS = .7 mm/sec

$\Delta t = -143\ \mu sec$

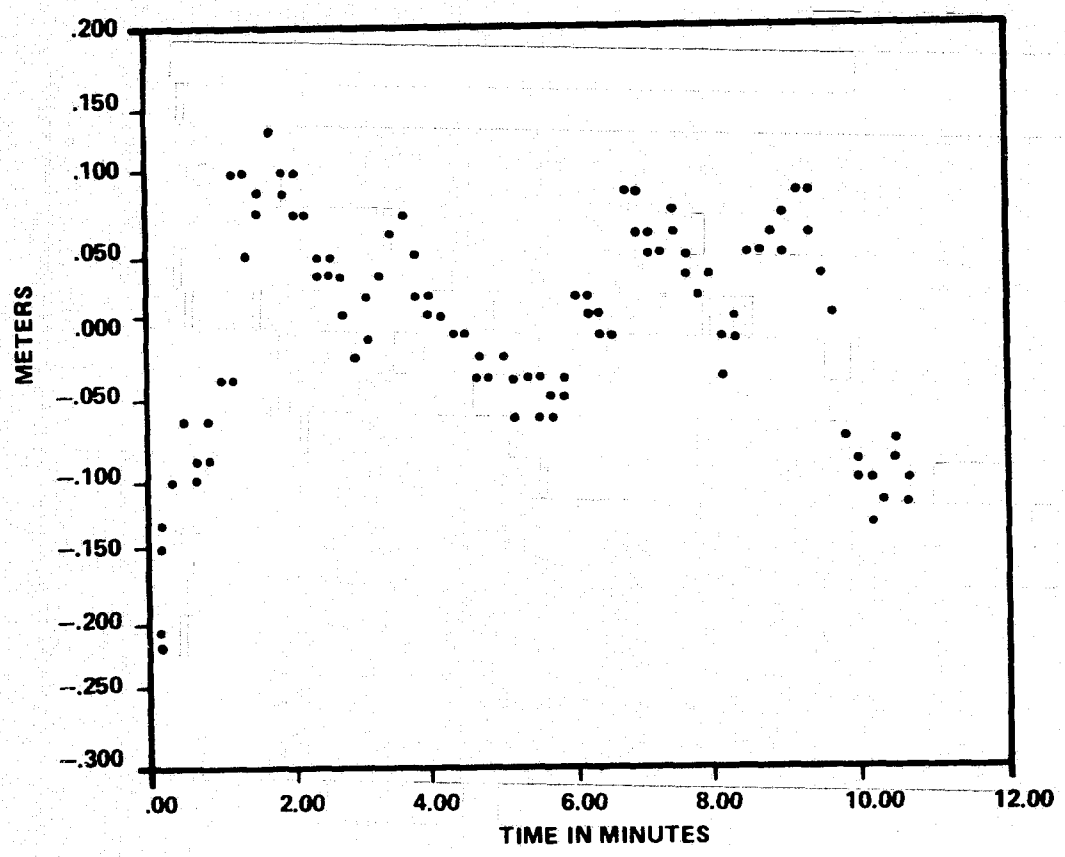

Other passes studied tended to yield similar results; the integrated ranges could always be reduced to a very low noise (1-3 cm RMS) data set by fitting an error model whose terms accommodated the effects of the ionosphere. Conversely, correction on the basis of a priori error term estimates yielded systematic error patterns grossly similar to those predicted by cursory ionospheric modeling. Uncertainty levels in both the ionosphere and the radar models indicate that the results are consistent.

SECTION 4.0
CONCLUSIONS

The primary objective of the GEOS-3 spacecraft C-Band Experiment was defined in the GEOS-C Mission Plan as,

> "To better determine the absolute accuracy of instrumentation radar systems, develop refined methods of calibrating these systems, and improve the techniques employed in processing the associated data."

This study has directly addressed that objective and made significant contributions to its achievement.

The integrated Doppler range technique has proven itself a sensitive and useful tool for resolving systematic errors and aiding in the calibration of coherent C-Band radars. In addition to producing extremely low noise range data, the potential for resolving the systematic error pattern present in a single station single pass orbital solution using biased range data may lead to an entirely new technique for calibration of C-Band radar bias errors. The range bias error is the single most limiting error in the use of C-Band radar data for geodetic work.

In the course of this study refinements made to the preprocessing procedures for conventional C-Band ranges significantly reduced their noise and systematic error. In particular, the AGC-based beacon delay variation is an important correction necessary in all future precision reduction of such data. Table 4.1 summarizes the calibration techniques developed or utilized in this study.

The limiting factor in reliable elimination of systematic error in the integrated range data is the availability of very accurate estimates of the radar error parameters, especially the servo lag coefficient and ionospheric refraction effects. The elimination of all systematic error from a range data set with essentially negligible noise is a difficult task which will extend traditional radar calibration techniques far beyond the domain in which they are ordinarily applied.

TABLE 4.1. COHERENT C–BAND CALIBRATION TECHNIQUES

NOISE REDUCTION

- NON–RECURSIVE POLYNOMIAL FILTER TO REDUCE RADAR RECORDED DATA RATE (APPLIED TO RANGE AND RANGE RATE DATA).

SYSTEMATIC ERROR REDUCTION

RANGE DATA

- PRE– AND POST–MISSION RANGING TO SURVEYED TARGET.
- SIGNAL STRENGTH DEPENDANT BEACON DELAY VARIATION.
- SERVO LAG CORRECTION.

RATE DATA

- TIMING ERROR (PRI/2).
- ONE LINE UP/ONE LINE DOWN BIAS ESTIMATION TECHNIQUE.
- INTEGRATION INTO PSEUDO–RANGE MEASUREMENTS.

Finally, the availability of two colocated ranging data sets with equal but opposite ionospheric refraction effects should provide the opportunity for competitive ionospheric model evaluation and other ionospheric studies.

REFERENCES

(1) Wells, W.T. and Guard, K., "Millimeter Range Precision from C-Band Radar CSP Measurements," presented to the Fall Meeting, American Geophysical Union, San Francisco, California, December 1970.

(2) Selser, A.R., "GEOS-C C-Band Transponder Prelaunch Calibration and Test Data," NASA TM X-69361, February 1976.

(3) Martin, T.V., et. al., "GEODYN Systems Description," EG&G/Wolf Research and Development Group, Final Report, Contract NAS 5-22849, August 1976.

(4) "Mathematical Description of the ORAN Error Analysis Program," Wolf Research and Development Corporation, Planetary Sciences Department Report No. 010-73, September 1973.

(5) Gerald, C.F., "Applied Numerical Analysis," Addison-Wesley Publishing Company, 1970.

(6) Goad, C.C., "Wallops Island Tropospheric Refraction Study and Analysis," Wolf Research and Development Corporation, Report Number 004-74, July 1974.

(7) Krabill, W.F. and Demsey, D.J., "C-Band Radar Pulse Doppler Error, Its Discovery, Modeling, and Elimination," NASA TM 69366, February 1978.

APPENDIX A
STEADY-STATE SERVO ERROR MODEL

Radar tracking system output does not consist of instantaneous, uncorrelated measurements but rather the sampled output of a servo loop. Where a laser ranging device uses measured round trip time-of-flight as the basis for its output range measurement, the radar system uses the deviation of this quantity from its expected value (in the sense of range gate position) to update its servo. At any given instant in time the range servo is not likely to agree with the last instantaneous ranging "measurement," nor should it if its output is to have a reasonable noise level.

All realizable (finite bandwidth) servomechanisms lag. The choice of bandwidth is usually a tradeoff involving noise reduction, dynamic response, and stability. Steady-state lag error in servomechanisms is generally modeled (1) as:

$$\epsilon(t_i) = \frac{\theta_i}{K_o} + \frac{\dot{\theta}_i}{K_v} + \frac{\ddot{\theta}_i}{K_a} \quad \cdots$$

where θ_i and its derivatives represent the input signal or function to the servo. The constants K_o, K_v, and K_a are servo design constants and figures of merit. Type I servos model only the input signal θ, and lag to first order with $\dot{\theta}$. Type II servos, such as the DIRAM range machine and the Coherent Signal Processor in the Wallops Island AN/FPQ-6, model both θ and $\dot{\theta}$, and lag to first order with $\ddot{\theta}$. Thus, the determining factor for first order lag in both systems is K_a, as shown in Table A-1. (For both systems in all bandwidths K_o is infinite and $K_v > 10^5$.) (2)

Figure A-1 illustrates typical GEOS-3 dynamics through a given horizon-to-horizon high elevation pass. The DIRAM range tracker lag error should go as the $\ddot{R}$ function* divided by K_a, usually 200. In other words it will lag approximately 25 cm at maximum acceleration. The Coherent Signal Processor operates on range rate and lags to first order as $\dddot{R}$ (jerk) divided by its K_a, ordinarily 27. It would typically lag 1-2 cm/sec at peak $\dddot{R}$ for a high elevation pass. The integrated CSP ranges, however, contain the integral of this $\dddot{R}$-dependent lag and hence, like the DIRAM ranges, will lag as $\ddot{R}$ albeit with a considerably lower K_a of 27, corresponding to a 2 meter effect in a high elevation pass.

REFERENCES

(1) Barton, D.K., Radar Systems Analysis, Prentice-Hall, Inc., 1964.

(2) Dempsey, D.J., RCA Surface and Missile Radar Division, Moorestown, N.J., personal communication, February 1977.

*In conventional (O-C) residual space the pattern is reversed and the lag effect is "bucket shaped."

TABLE A–1.

FPQ–6 DYNAMIC LAG COEFFICIENTS

DIRAM RANGE TRACKER

BW SETTING	1–5	6	7	8	9	10	11	12
K_a	2.2	6.5	20	75	200	1250	1790	3350
					↑ Normal Operation			

COHERENT SIGNAL PROCESSOR

FINE LINE FILTER BW	5 Hz	15 Hz	40 Hz	160 Hz
K_a	1	27	225	3000
		↑ Normal Operation		

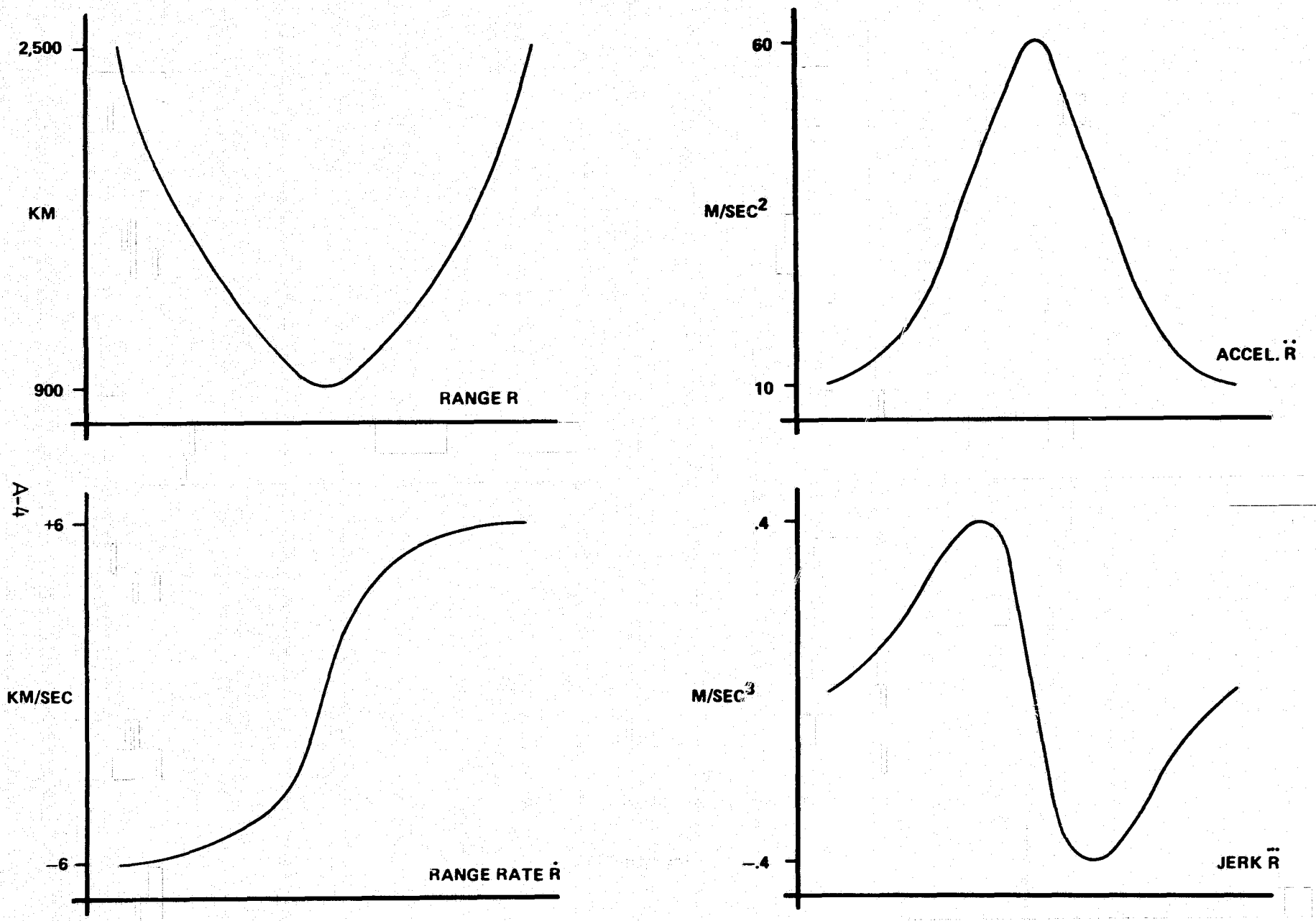

FIGURE A-1. TYPICAL GEOS TRACKING DYNAMICS

APPENDIX B
LEAST SQUARES SOLUTION FOR ERROR MODEL TERMS

The four parameter error model for integrated range residuals was fit to the residuals in the conventional least squares sense. The model

$$\Delta R_i = a_0 + a_1 \dot{R}_i + a_2 (t_i - t_o) + a_3 \ddot{R}_i$$

where

ΔR_i = ith integrated range residual

a_o = offset or bias; error in the constant of integration

a_1 = relative timing error between the CSP and DIRAM systems

a_2 = range rate measurement bias in the CSP system

a_3 = 1st order lag coefficient; $\frac{1}{K_a}$; see Appendix A

$\dot{R}_i$ = range rate at ith point

$\ddot{R}_i$ = range acceleration at ith point

$(t_i - t_o)$ = elapsed "integrator time" at ith point.

leads to normal equations which in matrix form require:

$$\begin{bmatrix} a_0 \\ a_1 \\ a_2 \\ a_3 \end{bmatrix} = \begin{bmatrix} \sum_i \left(\frac{\partial \Delta R_i}{\partial a_0}\right)^2 & \sum_i \frac{\partial \Delta R_i}{\partial a_0}\frac{\partial \Delta R_i}{\partial a_1} & \sum_i \frac{\partial \Delta R_i}{\partial a_0}\frac{\partial \Delta R_i}{\partial a_2} & \sum_i \frac{\partial \Delta R_i}{\partial a_0}\frac{\partial \Delta R_i}{\partial a_3} \\ & \sum_i \left(\frac{\partial \Delta R_i}{\partial a_1}\right)^2 & \sum_i \frac{\partial \Delta R_i}{\partial a_1}\frac{\partial \Delta R_i}{\partial a_2} & \sum_i \frac{\partial \Delta R_i}{\partial a_1}\frac{\partial \Delta R_i}{\partial a_3} \\ & & \sum_i \left(\frac{\partial \Delta R_i}{\partial a_2}\right)^2 & \sum_i \frac{\partial \Delta R_i}{\partial a_2}\frac{\partial \Delta R_i}{\partial a_3} \\ & & & \sum_i \left(\frac{\partial \Delta R_i}{\partial a_3}\right)^2 \end{bmatrix}^{-1} \begin{bmatrix} \sum_i \frac{\partial \Delta R_i}{\partial a_0}\Delta R_i \\ \sum_i \frac{\partial \Delta R_i}{\partial a_1}\Delta R_i \\ \sum_i \frac{\partial \Delta R_i}{\partial a_2}\Delta R_i \\ \sum_i \frac{\partial \Delta R_i}{\partial a_3}\Delta R_i \end{bmatrix}$$

The lower diagonal elements in the symetric matrix have been omitted for clarity. Computationally we find from the model

$$\frac{\partial \Delta R_i}{\partial a_0} = 1$$

$$\frac{\partial \Delta R_i}{\partial a_1} = \dot{R}_i$$

$$\frac{\partial \Delta R_i}{\partial a_2} = (t_i - t_0)$$

$$\frac{\partial \Delta R_i}{\partial a_3} = \ddot{R}_i$$

The fitting process, implemented in an existing residual analysis program (GEORGE) of the GEODYN system, was thus largely a matter of summing the normal matrix entries and one 4 x 4 matrix inversion. The necessary range second derivative estimates ($\ddot{R}$) were produced by twice applying a fifth order central difference numerical interpolation scheme to the smooth, calculated range data available on the orbit determination program's output tape.